

Article

Fatigue Strength Analysis of a Prototype Francis Turbine in a Multilevel Lifetime Assessment Procedure Part III: Instrumentation and Prototype Site Measurement

Eduard Doujak ^{*} , Anton Maly , Julian Unterluggauer , Franz Haller , Michael Maier, Christian Blasbichler and Simon Stadler

Research Group, Fluid-Flow Machinery, Institute for Energy Systems and Thermodynamics, TU Wien, Getreidemarkt 9/302, 1060 Vienna, Austria; anton.maly@tuwien.ac.at (A.M.); julian.unterluggauer@ait.ac.at (J.U.); franz.haller@tuwien.ac.at (F.H.); christian.blasbichler@tuwien.ac.at (C.B.)

* Correspondence: eduard.doujak@tuwien.ac.at; Tel.: +43-1-58801-302404

Abstract: Part I of this series of publications addressed the background and fundamentals of the lifetime assessment of prototype Francis turbines. Part II concentrated on the developed methods of numerical calculation and assessment procedures. The present contribution (Part III) deals with the instrumentation and the metrological range of the assessment procedure. The most important sensors, measurement tools, and data acquisition units are presented (background). The instrumentation of the prototype Francis turbine is used, on the one hand, for machine unit monitoring and plant operating and, on the other hand, for generating measurement data to validate and adjust/correct the numerical simulations. Measurement data form the basis for further evaluations at various levels. A wide variety of measured variables are required to carry out the remaining lifetime of a component using fatigue analysis. Those variables include pressure and acceleration signals, vibration monitoring, and strain gauge applications for mechanical stress analysis. The available measurement signals are divided into groups based on the developed method. Thus, already-available data from the control room are compared with machine monitoring and temporarily measured data. The correlation of all available data is essential today to determine an exact idea of the occurring flow phenomena and their effects on the mechanical stresses on the component. This interaction of the different data sources and, subsequently, the use of selected quantities for the numerical calculation are part of the newly developed concept for fatigue strength analysis of mechanical components of a turbine unit (methods). The results of this journal article are divided into the discussion of the necessary instrumentation and mounting of the sensors and into the evaluation, presentation, and interpretation of the measurement data. In addition, a fatigue strength assessment is made at the position of the strain gauges. These results serve as a basis for validating the numerical stress calculation. It is worth mentioning that the validation of the numerical results and the discussion of the deviations and error consideration is carried out in Part IV of this publication series (results). This journal article of the series on condition assessment of prototype Francis turbines ends with a discussion of the results and conclusions for further data processing (conclusion).

Keywords: hydropower; hydraulic turbines; lifetime assessment; multilevel procedure; measurements



Citation: Doujak, E.; Maly, A.; Unterluggauer, J.; Haller, F.; Maier, M.; Blasbichler, C.; Stadler, S. Fatigue Strength Analysis of a Prototype Francis Turbine in a Multilevel Lifetime Assessment Procedure Part III: Instrumentation and Prototype Site Measurement. *Energies* **2023**, *16*, 6072. <https://doi.org/10.3390/en16166072>

Academic Editor: José António Correia

Received: 1 July 2023

Revised: 1 August 2023

Accepted: 9 August 2023

Published: 19 August 2023



Copyright: © 2023 by the authors. Licensee MDPI, Basel, Switzerland. This article is an open access article distributed under the terms and conditions of the Creative Commons Attribution (CC BY) license (<https://creativecommons.org/licenses/by/4.0/>).

1. Introduction

The present paper is part of a series of several publications on the subject of fatigue strength analysis of prototype Francis turbines in a multilevel lifetime assessment procedure. PART I [1] contains the chosen approach's developed method and primary considerations, while PART II [2] is dedicated to the numerical approach. PART III presents the required sensor installation in the hydropower plant and the analysis based on measured data. References between the individual parts are repeatedly used to remain focused on the

essential core of the respective paper. The explanations and results in this paper refer to hydropower plant 2, described in detail in SECTION 2.2. of PART II [2].

This introduction aims to provide a concise historical overview of metrological investigations conducted in detecting flow phenomena relevant to damage in hydraulic machines, explicitly focusing on the lifetime analysis of Francis impellers.

With the advent of the liberalization of the European electricity market and the rise of new renewable energy sources (such as wind and photovoltaic), hydropower faces the challenge of operating its machines in off-design operating points. Francis and pump turbines are particularly susceptible to this mode of operation, as their runner blades cannot be adjusted to accommodate the altered flow regime. Consequently, early investigations were carried out to understand the flow phenomena occurring in these unconventional operating points. Detailed studies have been and continue to be conducted on flow separation, residual swirl leading to vortices and cavitation phenomena. As early as 2007, Ref. [3] demonstrated how blade trailing edge separation and the classical Von Karman vortex shedding frequency associated with it could lead to resonance problems and crack formation. Ref. [4] also reported on crack initiation in a Francis runner after in situ repair. At that time, the phenomenon of the draft tube vortex was known, but not its effects on crack initiation and, thus, on the component's lifetime. Metallurgical investigations were, therefore, carried out in addition to calculations. Blade failure was attributed to part-load operation and unfavorable flow conditions. A key issue in determining blade cracks in the fatigue strength simulation are the frequencies and amplitudes of the dynamic loads that occur, as shown by [5]. The first approaches to consider those effects already at the design phase were reported by [6] in 2012. Recent investigations on the laboratory test rig model [7] show that for this flow phenomenon, not only does the already known rotational frequency of approximately $(0.2 - 0.4) \cdot n$ occur, where n represents the rotational speed of the Francis turbine, but also higher proportions resulting from the self-rotation and the shape of the vortex. These considerations of unique flow phenomena allow the identification of individual frequencies from an overall frequency spectrum of the machine.

The first metrological and numerical investigations of the various operating points also began during this period [8]. In the beginning, these studies focused on the challenges at the transient operating points, such as speed-no-load or start and stop of the machine, since this was assumed to have the most damaging influence on the remaining lifetime of a Francis turbine [9]. In order to study these influences better, laboratory tests on model turbines were conducted. In particular, the shutdown of a turbine with a short-term increase in speed and the associated dynamic stresses on the runner represents a wide range of investigation possibilities. Ref. [10] is dedicated to the associated pressure fluctuations and mechanical stresses in this context and presented initial results in 2014. In parallel, the investigations of dynamic stresses continued and focused on a wide variety of load points [11,12]. According to current theories, this is important, since dynamic stresses are responsible for determining the remaining lifetime. However, the first studies were conducted on laboratory test rigs, which again have a scaling problem. A general study on this is presented in [13].

The quintessence of these investigations results in predicting the lifetime of Francis turbines under the previously mentioned conditions. For more than ten years, the influence of various parameters on the residual lifetime has been investigated. Suppose a deviation is made from the classical design of water turbines according to the medium stress concept in the direction of fatigue strength. In that case, entirely new challenges arise in determining dynamic stresses. As already shown in Part I of this paper series, different flow phenomena occur in the individual load steps and cause those pressure fluctuations, which in turn lead to dynamic mechanical stresses responsible for the lifetime reduction. This is shown in the study [14] from 2012 and subsequently from 2014, presented in [15]. Mechanical stresses depend on the size of the structure, since the mass, damping, and stiffness matrix cannot be easily scaled. Many examinations have been conducted on prototype machines [16,17].

There is still a distinction between whether strain gauge measurements exist directly on the runner [18] or not.

The subject of several review papers is the influence of singularly damaging flow phenomena and their combinations on the operation of a Francis turbine at different operating points. For example, the transient effects, such as start–stop or load rejection of a machine, are addressed in [19]. How these effects can be transferred from the fluid domain to the component structure and which procedures or methods have been applied to date are described in [20]. These mathematical procedures and methods require solid validation, which can only occur in prototype hydropower plants to avoid scaling effects between the model and prototype runner. Experimental tests and measurement procedures in real plants are described in [21]. The literature shows that the distinguished influence of the draft tube vortex on the lifetime of Francis turbines has recently become a topic of interest. This flow phenomenon plays a significant role, especially in Francis turbines with a higher specific speed n_q . The possibilities of detection in hydraulic machines are described in a review paper [22]. The publications cited give a comprehensive overview of the methods and procedures used in the field of flow patterns and possible effects on the element structure.

In recent years, the need for stress–strain measurements on the runner under actual operating conditions has been acknowledged in order to validate the calculation methods and to determine the associated vibration modes and natural frequencies in the frequency domain. The possibilities of such measurements are, of course, limited and not feasible for every runner. A suitable hub design is needed to accommodate the data logger and power supply and to protect them from the flow. In addition, the boundary conditions for the strain gauges are extremely harsh, so they can only be in use for a short time period. Examples of such plant measurements with strain gauges and their evaluations are presented in refs. [23,24]. In this context, of course, the issues of “oscillating water masses”, stiffness effects of the labyrinth seals, and system damping due to the lubricant film thickness in the bearings must also be taken into account. While these factors are automatically included in the prototype measurements, they represent an enormous challenge in the development of computational models.

This short literature review shows that there is still room for further method development and research work about the lifetime assessment of Francis turbines. Especially in the area of turbine measurement technology, data acquisition and storage, on-site processing, and integration into the operating SCADA system, many questions are still unanswered. The sampling rate and automated detection of damage mechanisms will still need to be investigated for longer. It can already be seen that only a combined approach of calculation and measurement will lead to the goal. Accordingly, further plant measurements on selected machine units are of utmost importance.

This paper series is dedicated to this comprehensive question, but it is so voluminous that it has to be divided into several parts. This articles content includes the plants metrological equipment for the validation measurement, the measurement procedure, and the presentation and evaluation of the results. The structure is as follows.

Section 1 provides a literature review of the latest publications on the experimental validation of a Francis turbine lifetime assessment. An emphasis on the proposed evaluation method going beyond the State-of-the-Art shows the heuristic approach focusing on the metrological part (see Figure 1).

Section 2 describes the metrological process in the selected hydropower plant, consisting of the measurement site identification, sensor selection and application, and measurement procedure to obtain the necessary data to validate the calculations. In addition, sensors are placed in those areas and cross-sectional planes, which will be needed as boundary conditions for the numerical simulation later.

In Section 3, the measurement results at several operating points and different aspects are presented. Correlations of distinct sensor data illustrate a singular flow phenomenon from different points of view and under the influence of air injection. Furthermore, the

lifetime at strain gauge spots is evaluated. Extrapolation in the direction of the hotspot is omitted because the concept of stress-intensity factors is too imprecise. The conventional approach is considered critical in this case and will be explained in more detail in Section 3.3.2.

Section 4 discusses the topic of sensor selection and a possible extension of the diagnostic system. Based on the predefined sensor groups and the subsequential data time series as well as frequency spectra, a correlation matrix can optimize the selection of measurement signals for a diagnostic system. A substantive discussion on the stress-intensity factor rounds out the chapter.

Section 5 deals with the conclusions of the findings and gives recommendations for further procedure.

In Appendix A, the sensor installations at the hydropower plant are shown. Additionally, application notes and sensor characteristics are presented. In order not to distract the paper content too much, it was decided to add this information at the end within the Appendix A.

Beyond the State-of-the-Art Investigations—The Transient Assessment Model

Figure 1 shows the content of this paper quite clearly. The upper green area represents the simulation level, while the red area in the figure’s lower half represents the process’s metrological part. It is clear from this figure that both numerical simulation and metrological validation are necessary for determining the service life of the component (Francis turbine). This necessity and interplay between simulation and measurements will be described and discussed in more detail later on.

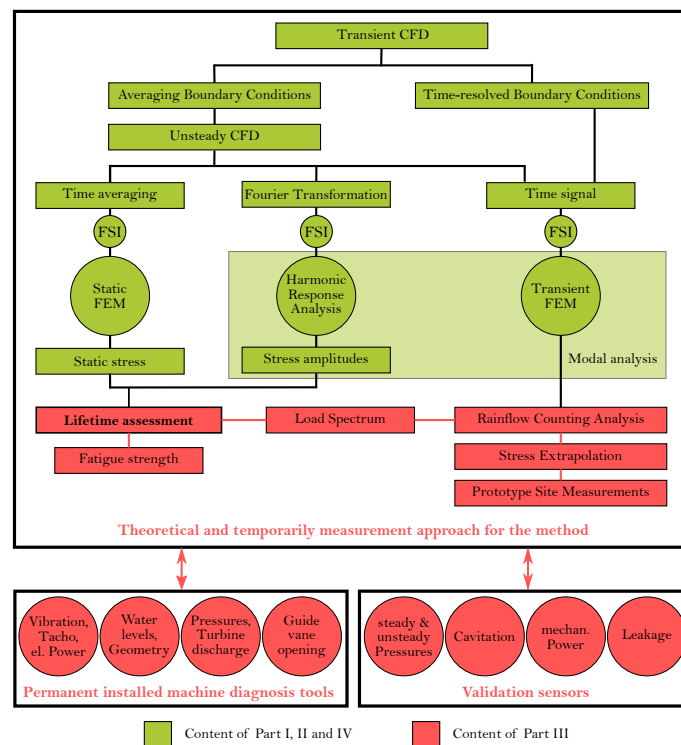


Figure 1. Measurement path of assessment method.

As already presented in PART I [1] and PART II [2], the transient mechanical stress calculation is a new approach to the determination of the lifetime of a Francis turbine. Especially the time-resolved boundary conditions need reliable metrological validation. Therefore, boundary conditions, monitoring points and simulation results must be validated with measurement data in the best possible way. Since measurement and simulation always diverge, performing an accurate error analysis with subsequent uncertainty evaluation is essential.

Diverse data sources can be used, e.g., operational data processed in a SCADA system or additionally installed monitoring sensors providing mechanical protection for the machine. In some cases, however, additional sensors are needed to provide the necessary time series data for the validation. These additionally required sensors can be subdivided again into those that can only be used temporarily. Moreover, those sensors can be mounted permanently on the outside of the machine set. This group of sensors also has the potential to be included in the list of operational data if it proves helpful.

The selection of the required sensors and measuring devices, as well as the further processing of the obtained data, is described in this article. Due to the large number of different flow phenomena which can influence the operation of the machine and are responsible for the decrease in service life, adapted measurement variables and sampling rates are used. In the context of the method development for determining the residual lifetime of a component, it primarily concerns the collection of the necessary signals and their temporal resolution. In many cases, the existing operating data is too coarse in its granularity to be used meaningfully in method development. Therefore, some operating signals are recorded additionally in higher resolution to ensure proper processing. In the first step, a load increase method is applied to investigate the behavior at different operating points in more detail. Subsequently, monitoring systems for continuous operation could be developed from this.

2. Measurement Process

The focus of the underlying research project is to establish the correlation between machine operation and lifetime for all operational points. As shown previously and as documented by the cited publications, the behavior of the machine unit relates to different flow patterns and resulting loads. The question arising at this stage is the proper instrumentation to cover all different instabilities and loads to get an overall impression of the condition of the machine or its components. One has to take into account that various flow phenomena would require different measurement techniques to examine their influence. Moreover, the question whether important investigation parameters can be measured directly or indirectly has to be answered. Another important point is the occurrence of more than one different flow phenomenon at one operation point, as shown in TABLE 2 in PART I [1], thus making the prototype measurement and data interpretation much more difficult during post-processing.

Based on the already-performed prototype measurements, the selected sensor installation and measurement procedure is discussed to show the complex task of attempting to collect the correct data at the proper position. A well-prepared instrumentation and workflow plan is essential for the acquisition of useful data.

2.1. Instrumentation Overview and Sensor Application

As mentioned in the introduction, all figures, interpretations, and results refer to hydropower plant 2, which has already been described in detail in SECTION 2.2 of PART II [2] of this paper series. This plant can be used as a representative for all other hydropower plants, as the installation of the measurement equipment can only be limited by the accessibility of the machine unit. However, all stress analyses and evaluations remain unaffected, and thus, retain their validity.

Figure 2 shows the different positions with their measurement signals at the machine unit and turbine cross section.

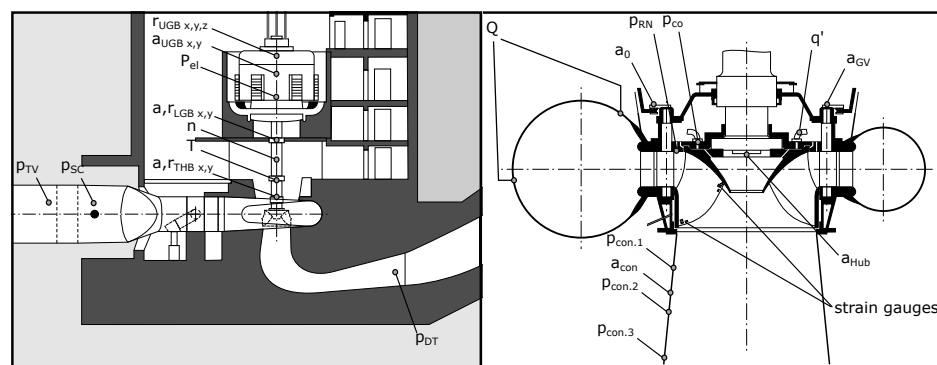


Figure 2. Sensor position and measurement signal plan.

To organize the multitude of signals, a suitable classification system based on the considerations above was developed.

- Permanent installed sensors to acquire operational data. Usually, those sensors measure operating variables, such as water levels, flow rates, drop heights, angle of the guide vanes, or electrical power. Mostly, they lack appropriate data granularity for the methodology as the sampling rate is rather low. However, they are still usable as CFD boundary conditions or to validate the global CFD-simulated parameters. The list of used sensors and their quantity is visible in the first block of Table 1. The data storage source is usually the server storage media within the SCADA system.
- Permanent machine diagnosis sensors. Permanent machine diagnosis consists of a set of various sensors which are attached to different components to measure the behavior directly or indirectly. The time series of the sensor signals are processed (for example, transfer into frequency domain) to gain more insight into the component condition to avoid unexpected breakdowns. These signals are also the base for any further developed maintenance strategy. The following positions on hydraulic machines or their operating parameters are already frequently considered for permanent machine diagnostics:
 - Detecting the position and vibration of the Runner [25,26]. The method detects some sources of error in the shaft line, such as off-design regions, imbalances caused by mass displacement or shaft misalignment, shear pin malfunctions, or vibrations at the guide vane apparatus and radial bearing problems.
 - Detecting vibrations and dynamic pressures at the head cover and/or the draft tube cone [25,26]. Erosion and abrasion phenomena, such as cavitation, sand particles, etc., damage the water-carrying components of a hydraulic machine and, thus, of course, the runner itself. They lead to material loss at particularly exposed locations or sealing gaps, and thus, reduce the efficiency of the machine unit. Progressive erosion even forces a shutdown and repair of the unit. Altered gap dimensions or clearances can lead to vibrations in housing parts. Acceleration sensors monitor vibrations at the head cover and the draft tube cone. Changes in the frequency or amplitude of those signals are used for monitoring and operating the machine unit.
 - Checking the seal ring gap. Labyrinth seals are used in Francis turbines to limit gap water flow and increase turbine efficiency. Sensors that monitor the sealing gap assist in machine monitoring in terms of efficiency.
 - Measuring Temperatures at Thrust and Guide Bearings. Failure sources, such as insufficient lubricant film thickness, mechanical overload, or bearing material fatigue, lead to difficulties in keeping the bearing oil

film stable, and therefore, cause a temperature increase in hydraulic oil and the bearing itself.

- Detecting the oil film thickness at thrust bearings.
A collapsing oil film thickness damages the thrust pads in axial bearings, and thus, inevitably stops the machine unit. If this is not detected and corrected in time, bearing or even damage to the rotor is unavoidable. Appropriate installed vibration displacement sensors prevent this by measuring the axial bearing distance or the oil film thickness.
- Detecting vibrations in the stator frame of a generator [25,26].
The generator of a hydraulic machine set is subject to many magnetic and thermal cycles during its lifetime, which can lead to the loosening of parts and vibrations. These occurring vibrations as indicators of approaching damage to the generator stator can be detected using accelerometers and implemented in the unit's machine diagnostics.
- Detecting vibrations in stator bars and end windings [25,26].
Stator bars and subsequential end windings are subject to electromagnetic, mechanical, and gravitational forces during the regular operation of a hydroelectric generator, which can cause the stator bar splice to become detached. The consequences are vibrations and insulation losses, which in turn cause the unit to shut down and result in a longer repair time.
- Checking the air gap between the generator rotor and stator.
The air gap between the generator rotor and stator is an essential measure of the efficiency of a hydroelectric generator. The smaller the air gap is, the lower the losses in this component. Therefore, measuring the air gap is an important indicator for the quality assessment of a hydropower generator. Depending on the design, between one and sixteen sensors are used around the circumference of the generator stator. They measure instantaneous values, subsequently treated as statistical values, such as min, max, and average values. Furthermore, the roundness of the rotor, as well as the stator, can be verified.
- Monitoring partial discharge behavior at the generator.
Partial discharge measurements are used to determine the quality of the insulation of a hydropower generator. These are based on the corona effect and represent local electrical discharges. They can occur in cavities within the insulation system or at microcracks in the insulation itself. The number of detected partial discharges between the rotor and stator measures the insulation quality and can, therefore, be integrated into a modern maintenance management system. However, no standard for comparative values exists, so company or operator know-how is needed.
- Monitoring operational parameters.
In the SCADA system of modern hydropower plants, necessary operating variables are recorded and stored. These are parameters such as level heights of reservoirs or river stretches, rotational speed, power output, various generator voltages, bearing temperature, pressures, and positions at the valves. These measured variables are sampled at a higher sampling rate, but are then usually only stored at 1 Hz or less in the long-term storage systems of the power plant operators.

Today, these measurement techniques and related sensors are correlated in terms of condition monitoring. Additional information on the powerhouse control system and market information leads to developing enhanced maintenance strategies such as predictive maintenance. In the present research study, the used permanent monitoring sensors are listed in block 2 of Table 1. The data storage source is mostly a separate server structure media and some processed data are sometimes exported to the SCADA system. However, usually, these signals are separately processed as their main purpose is the machine protection against mechanical disruption.

- Temporary measurements for component assessment.
Temporarily direct attached sensors for component assessment determine the mechanical stresses utilizing strain gauges or runner properties, such as the natural frequency by using accelerometers. So-called direct measurement methods are used here. This form of measurement data determination should be considered first, as far as possible, because they provide the most original values. However, the application of such sensors is limited in hydraulic machines, as the parts in contact with water do not provide an ideal environment for using this direct measurement method. The dwell time of such sensors is limited to a few hours and can only be provided for initial measurements. The data storage is usually a data logger, as telemetry systems are most likely to be used in the presence of a hollow shaft. Very rarely, the signal from the telemetry system is transmitted via the waterway, as this is very complex and costly. Moreover, it only makes sense to use it with larger turbine units. In the present research project, strain gauges and acceleration sensors were installed on the impeller and data sampling was carried out using a data logger. The storage medium was a conventional SD card.
- Temporary validation sensors.
This group uses sensors that can be externally attached to the machine unit. They serve as boundary conditions for the CFD simulations and validation values for the integral calculation parameters or as a direct comparison with monitoring points. The number and mounting options on the machine depend very much on accessibility. In addition, these sensors can be included in the list of operating data if this proves helpful. A unique feature of this research project was the non-contact measurement of the mechanical torque on the shaft. This was possible because there was a sufficiently long, exposed turbine shaft between the lower generator and turbine bearing. The background to this measurement is splitting the outputs ($P_{hydraulic}$, $P_{mechanic}$, $P_{electric}$), and thus, the possibility of separate efficiency consideration. This means the hydraulic efficiency can be determined separately for the first time. Furthermore, it is interesting to see to what extent existing flow phenomena are responsible for power fluctuations at the generator. Group 4 of Table 1 shows the number of sensors.

In total, a list of 29 parameters (see Table 1) comprising a quantity (*Qty*) of 53 sensor signals with different sampling rates should give the possibility to evaluate the behavior of the runner and guide vanes of the unit.

Table 1. List of measurement signals and usage.

No.	Signal	Qty	Position	Signal Type	Usage
PERMANENT OPERATIONAL DATA					
1	z_{HW}	1	head-water level	geodetic height in m	operating point
2	z_{TW}	1	tail-water level	geodetic height in m	operating point
3	a_0	1	wicket gate	choke length in %	operating point
4	Q	1	in the spiral case	discharge in m^3/s	operating point
3	p_{TCV}	1	before turbine closing valve	pressure in bar	operating point
4	p_{SC}	1	at the spiral case	pressure in bar	operating point
7	p_{RN}	1	runner entry	pressure in bar	pressure distribution in side chamber
8	p_{CO}	1	turbine cover	pressure in bar	pressure distribution in side chamber
9	$p_{con.2}$	1	draft tube cone	pressure pos. 2 in bar	DTV, FSO, SPP
10	n	1	turbine shaft	speed in min^{-1}	operating point, mechanical power
11	P_{el}	1	generator	electrical power in MW	electrical power, efficiency

Table 1. Cont.

No.	Signal	Qty	Position	Signal Type	Usage
PERMANENT MACHINE DIAGNOSIS SENSORS					
12	$r_{THB_{x,y}}$	2	turbine bearing	displacement in x,y in μm	relative shaft vibration
13	$a_{THB_{x,y}}$	2	turbine bearing	velocity in x,y in mm/s	absolute bearing vibration
14	$r_{LGB_{x,y}}$	2	lower gen. bearing	displacement in x,y in μm	relative shaft vibration
15	$a_{LGB_{x,y}}$	2	lower gen. bearing	velocity in x,y in mm/s	absolute bearing vibration
16	$r_{UGB_{x,y,z}}$	3	upper gen. bearing	displacement in x,y,z in μm	relative shaft vibration
17	$a_{UGB_{x,y}}$	2	upper gen. bearing	velocity in x,y in mm/s	absolute bearing vibration
TEMPORARY MEASUREMENTS FOR ASSESSMENT					
18	<i>strain gauges</i>	15	runner	strain in $\mu\text{m}/\text{m}$	local stress in runner
19	a_{Hub}	1	runner hub	acceleration in m/s^2	DTV, SPP, ICV, shaft vibration
TEMPORARY VALIDATION SENSORS					
20	p_{DT}	2	draft tube end	pressure in bar	cavitation number
21	$p_{con.1}$	1	draft tube cone	pressure pos. 1 in bar	DTV, FSO, SPP
22	$p_{con.3}$	1	draft tube cone	pressure pos. 3 in bar	DTV, FSO, SPP
23	q'	1	collection pipe	discharge in l/s	leakage in side chamber
24	a_{con}	1	draft tube cone	acceleration in m/s^2	DTV, FSO, SPP
25	a_{GV}	2	guide vane	acceleration in m/s^2	leading edge cavitation (SPP)
26	$a_{THB_{x,y}}$	2	turbine bearing	acceleration in m/s^2	validation, absolute bearing vibration
27	T	1	turbine shaft	torque in Nm	mechanical power, efficiency
28	n	1	turbine shaft	speed in min^{-1}	validation, mechanical power
29	P_{mech}	1	turbine shaft	mechanical power in MW	mechanical power, efficiency

While the interpretation of the data gets complex by using the parameter list and its combinations, it is very interesting. Results will show if the research goals could be reached. The next step in line is the definition of a proper measurement procedure to guarantee that all points of the operating range are covered. For the fatigue evaluation of the runner, every load step, including the start–stop of the machine, is needed to calculate the proper load spectrum. The focus of the underlying research project was to determine the influence of the load shift and start–stop burden on the runner.

The application and main characteristics of the individual sensors are described in the appendix.

2.2. Measurement Procedure

Besides installing the sensors, the definition of an adequate measurement procedure is essential. As the focus is the evaluation of the dynamic loads during load shifting and start–stop of the machine unit, the procedure contains two different ways to start the machine. Figure 3 shows three separate peaks at the beginning of the procedure. The first start-up procedure (Test Start-Up) was a test to check the manual operation of the machine unit; the project team modified the second one (1. Start-Up) to lower dynamic loads. The third start-up (2. Start-Up) procedure corresponds to the regularly implemented one, which is optimized to reach fast synchronization times. Further load steps have been selected based on the hill chart and the experience of previous research projects. At lower part load regions the load steps were performed in steps of 3 MW, while around the BEP, steps were about 6 MW. In total, 13 load steps upwards and downwards have been part of the measurement procedure. The measurement time within one load step was between 5 and 10 min to ensure

sufficient data were acquired. The single ramps covered all operation regions, as shown in FIGURE 2 at [27], up to overload and down to minimum load again. Compressed air was injected during the measurements from overload to minimum operational point to stabilize the machine's behaviour. Towards the end of the measurement process, the machine was de-watered and operated at condenser mode to investigate the draft tube wave. Afterwards, the turbine was watered again, and a load rejection case was performed. Figure 3 shows the measurement procedure lasting about 4 h. Besides power output (P), discharge (Q), and guide vane opening (a_0), one can see that the measurement was performed at a constant head. This was to ensure that possible waterway oscillations would not influence the measurement. Therefore, the secondary unit was running at a constant load.

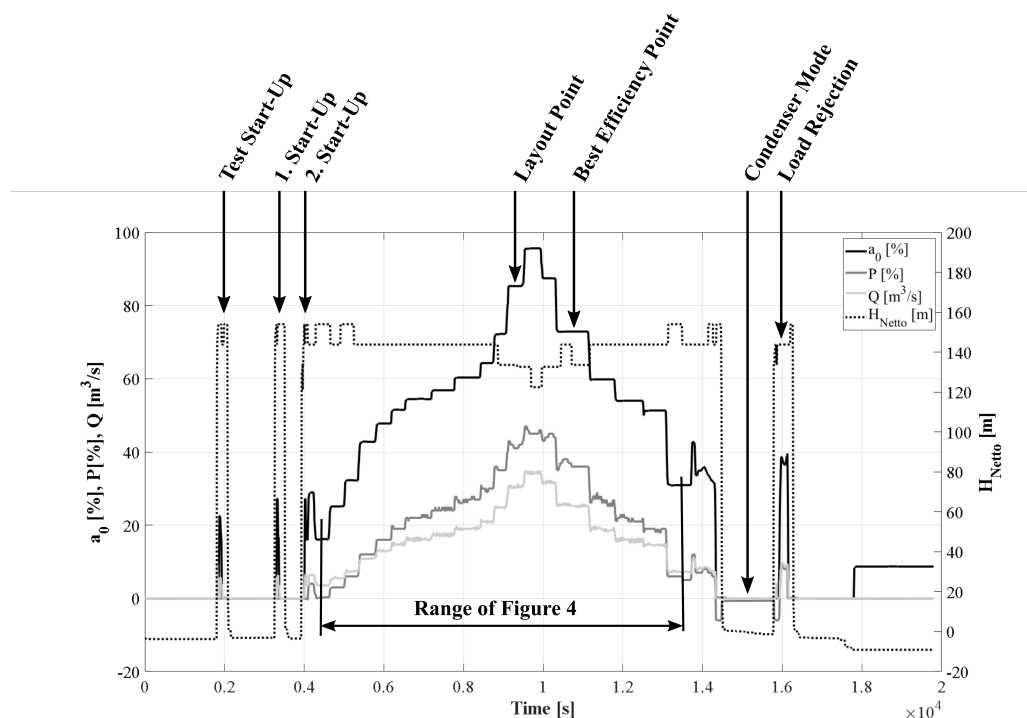


Figure 3. Measurement procedure.

Time-synchronous recordings were made of all sensors used during the measurement procedure. This is essential as it enables the exact correlation of the data afterwards. Marking the points at the hill chart of the turbine, one can recognise the line of operation along a constant head curve.

2.3. Data Processing

Data acquisition at such projects has to deal with different data sources looking at the four measurement signal groups from Table 1. The group of permanent operational data were taken from the existing operation management servers and provided by the operator as an ASCII file. The time interval, that is, the sampling rate of these time series data, was 10 Hz. Several data acquisition devices were used to obtain the remaining measurement signals.

Since some operational data had an inadequate time granularity, they were separately sampled with a digital data acquisition unit (DDAU III) at a higher sampling rate (6.4 kHz) to be accessible for later evaluation.

Due to the many analog and digital inputs of this unit, the shaft and bearing vibration signals of the permanent monitoring system could also be acquired at a sampling rate of 6.4 kHz.

The temporary signals from the strain gauges and the additional accelerometer were stored with a data logger mounted on the hub. The sampling rate for these sensors was 2 kHz.

The remaining temporary signals from Table 1 were recorded using a second digital data acquisition unit (DDAU III) with sampling rates ranging from 2 to 204.8 kHz.

For post-processing, all data were processed and pre-analyzed using MATLAB software (<https://matlab.com>). They were stored in a database using TSM technology to correlate multiple time series, then harmonized and subjected to Pearson correlation using VISPLORE software (<https://visplore.com/>). Thus, all signals in a correlation matrix could be examined for similar or opposite behavior.

3. Results

Due to the vast number of sensors and the long measurement time of approximately four hours, not all measurement data can be presented at once. In this paper, the authors focus on the following essential aspects of the hydraulic machine and time series data evaluation:

- Only different load steps of the grid-synchronised machine unit are investigated.
- The transient operating conditions, such as start–stop or load rejection of the machine, are not addressed, as these operating modes have already been published in the paper [28].
- In the load intensity tests, operating points with and without air injection were analyzed. The effects of these different operating modes on the lifetime of the Francis turbine are investigated in this part.
- An attempt is made to build up an exemplary sensor correlation matrix from the different sensor groups described above concerning the extension of the existing diagnostic system.
- Based on this, conformal data time series for detecting damage-causing flow phenomena within the machine unit is derived from the various sensor groups.
- The site measurement is conducted along a constant headline in the Hill Chart diagram and used for the subsequent lifetime prediction of the Francis runner. Other operational points are not considered at the moment. This will be part of the coming issues.

Considering the above list, focusing on two experimental aspects seems reasonable. The data time series, frequency analysis, underlying flow phenomena, and damage conditions are presented and interpreted based on these.

1. The first aspect being compared here is the different signal behavior in the part-load range and the best efficiency point. The selection was made due to power signal behavior in Figure 4. For more detailed information, see the description.
2. The second aspect apparent in this system is the injection of compressed air in the part-load range. Part-load points were measured with and without air injection during the measurement procedure. Figure 4 clearly shows this aspect. An attempt is made to quantify the effects of this air injection on the operation of the machine unit.

Figure 4 shows the measurement signals of the hydraulic, mechanical, and electrical power. The hydraulic power cannot be measured directly but is calculated and averaged from measured discharge Q and head H , the mechanical power has been determined according to Appendix A.4.6, and the electrical power has been taken from the operational data acquisition. The figure gives an impression about the time signal behavior at different load steps of the measurement procedure (see Figure 3 and description in Section 2.2). It shows that at very low loads, the hydraulic power correlates very weakly with the mechanical and electrical power. This is due to inaccuracies of the implemented Winter–Kennedy measurement for determining turbine discharge Q . Furthermore, a torque fluctuation can also be detected at this load range, which, however, does not seem to have a significant effect on the electrical power. This circumstance changes in the part load range of approximately 50–60%, where larger torque fluctuations become visible and power swinging of the generated electrical power occurs. As expected, the fluctuations are reduced again at the best efficiency and design point.

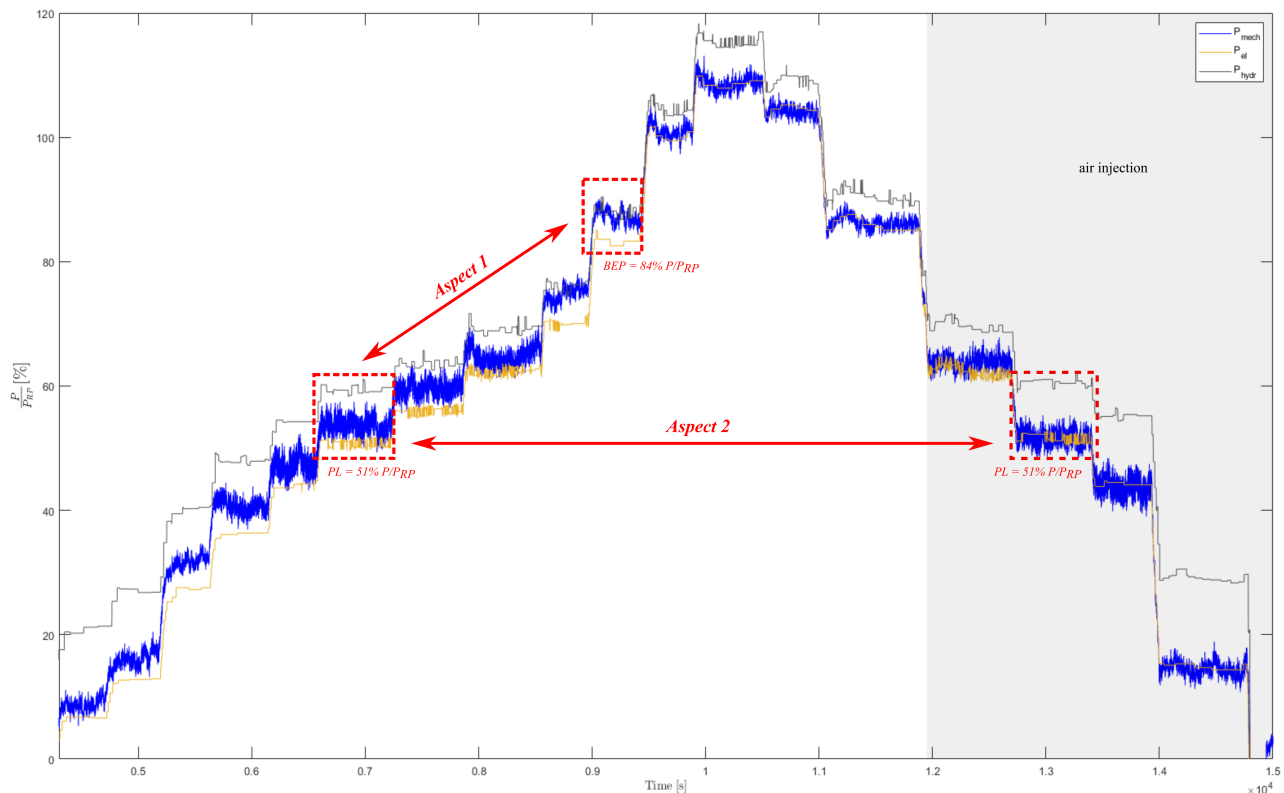


Figure 4. Time signals of hydraulic, mechanical, and electrical power.

In the context of aspect one, the load points of ($PL = 51\% P/P_{RP}$) and ($BEP = 84\% P/P_{RP}$) were defined and used for further evaluations. The second aspect to be discussed within the scope of this evaluation can be observed in Figure 4 on the right-hand side of the measurement procedure, where compressed air was injected into the turbine at an operating point of approximately 60% downwards in the area of the vaneless space. Some effects of this operation mode have already been presented in [29]. This paper attempts to illustrate and discuss the changes in operating conditions caused by the injection of compressed air within the measurement signals. Therefore, a distinction is made between UP and DOWN at the operating point ($PL = 51\% P/P_{RP}$). UP is operated without compressed air and DOWN with.

3.1. Examination Of Measurements (Aspect 1)

Since this part deals with determining the lifetime of a Francis turbine from prototype measurement data, the consideration of the component metrological data is of primary importance. In this case, the essential information can be obtained from the temporary sensors (strain gauges and accelerometer in the hub) since those sensors were installed directly on the runner. The behavior of the strain gauges during the load tests is shown in Figure 5. Furthermore, clearly visible is that the dynamic parts of the strain signals in the part-load regions are greater than those in the best efficiency point. Figure 5 shows the raw data obtained by the strain gauges located at the pressure side of the runner blade. More about the preliminary calculations and the positioning can be found in Appendix A.3.1 and in [30].

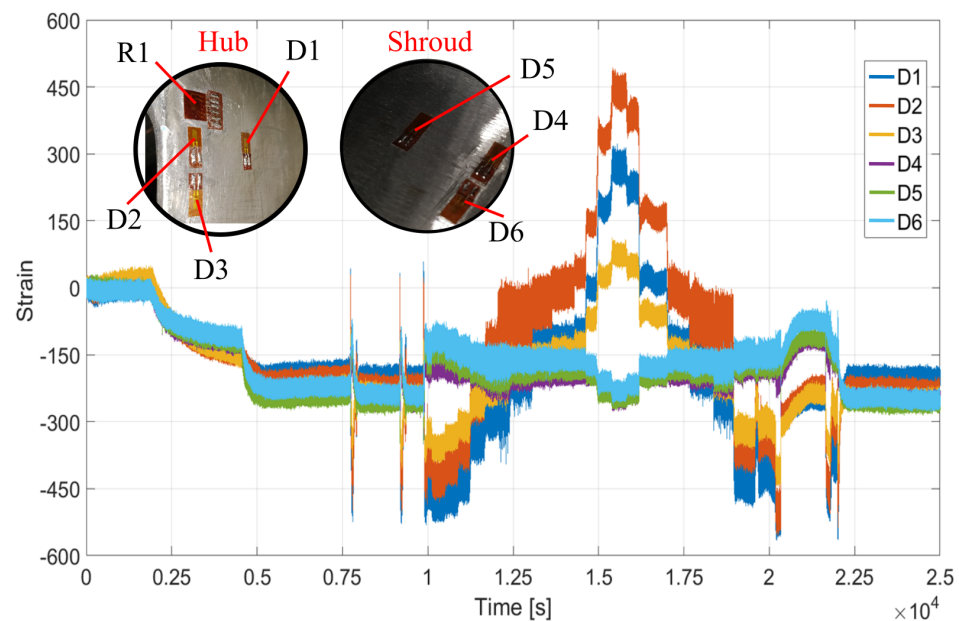


Figure 5. Time signals of mechanical stresses at different strain gauges during measurement; results of strain measurement for the pressure sided strain gauges.

Looking at the starting point of the strain signals in Figure 5, the refilling of the Francis turbine with cold water can be recognized. The strain gauges contract due to the temperature difference and obtain negative values, which are then used as a base for the starting sequence of the machine unit. The influence of start-ups is visible as high peaks in strains. Those transients will be investigated separately. After the SNL section, where the strain gauges at the shroud show a rising and those on the hub a more negative value, the strains change over the load steps. Hub strain gauges increase in value, whereas shroud ones decrease up to the maximum load. The strain values show the same behavior on the way down before load raising. The influence of air injection is not markable. From this point of view, it is challenging to justify air injection.

At the end of the measurement procedure, one can recognize that the strain values cannot fully recover. This means that during the measurement time, the strain gauges drift in their absolute values, having many different reasons. Those will be discussed in PART IV of this paper series. At the moment, this drift has to be considered and corrected at the conversion from strain to stress values.

Considering the theory from PART I, where individual flow phenomena were correlated in (PL and BEP) load-steps, it makes sense to identify the known frequencies within the measured data signals. For this purpose, specific signals were investigated in both the time and frequency domains. Those sensors that were temporarily mounted to the existing equipment are of particular interest. Since this group of sensors is available for inclusion as permanent sensors, they are used and evaluated here as reference sensors. Thus, the reasonableness of the sensor application is verified, and the data quality is checked. This is done by using sensor numbers 22 ($p_{con.3}$) and 26 (a_{THB_y}) from Table 1. Sensor number 29 (P_{mech}) has already been used as argumentation support in Figure 5.

When studying the signal fluctuations in the PL range, one will consider the presence of a DTV. The known DTV frequency is below the rotational frequency and is expected in the following signals.

The pressure signal of the second piezoresistive transducer $p_{con.3}$ is shown in Figure 6. On the left side, the machine is operating at the best efficiency point. One can see the signal in the time domain for 30 s. The pressure fluctuations are approximately ten times lower compared to the right side, where the machine operates in the part-load region.

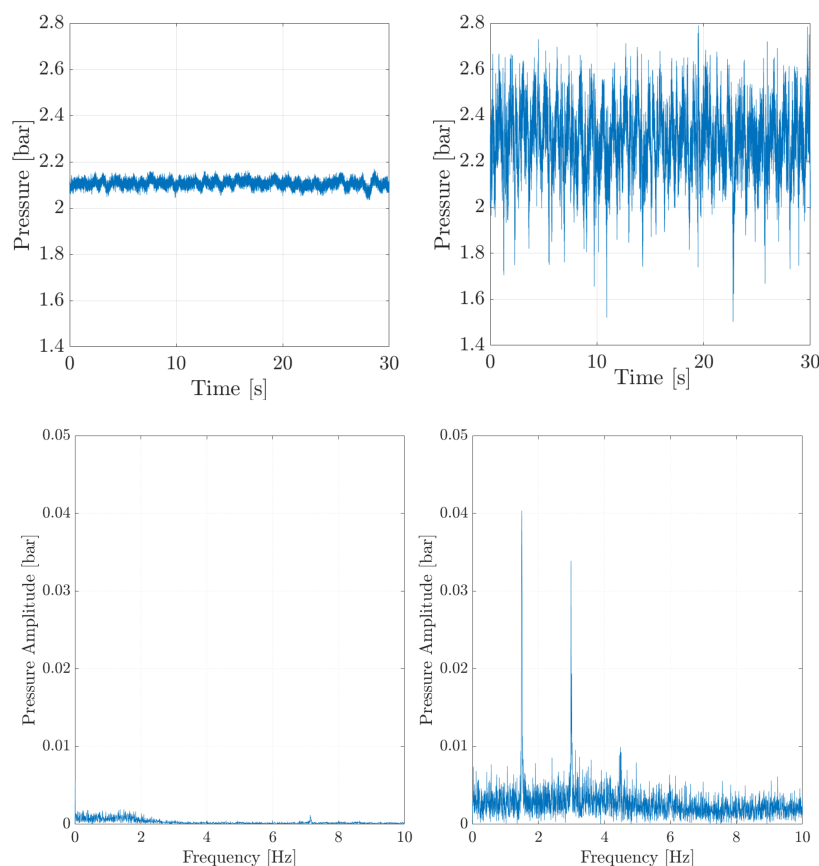


Figure 6. Pressure signal $p_{con.3}$ in the time and frequency domain at the best-efficiency point (BEP) (left) and part-load (PL) point (right).

Similar behavior can be observed in the frequency spectrum. The amplitudes at PL are also much higher than in the BEP. In addition, frequencies below the Francis runner rotational frequency of 7.14 Hz become visible. A DTV frequency of around 1.4 Hz is expected and detectable. Furthermore, some partial frequencies of 1.4 Hz can be identified, which are indicative of a split DTV and not a single one.

Another exciting aspect of the data analysis is the question of the effect of the DTV. As shown in Figure 4, the torque also fluctuates at this part-load point (PL), not just the hydraulic power. Accordingly, the influence on the orbit of the turbine shaft has to be discussed. The orbit represents the behaviour of the turbine shaft in the bearing quite well and is, therefore, important for determining proper concentricity.

Figure 7 shows the behavior of the turbine shaft in the area of the turbine bearing in both BEP (left) and PL (right). The orbit shape is shown for three revolutions. The BEP shows a conformal behavior of the turbine shaft and an oval orbit shape. This shape corresponds to the expectations at this load point. In the PL area, a different orbit behavior can be seen. Here, the turbine shaft is subject to specific radial forces in the bearing, which prevent an oval orbit shape. It is also subject to more significant deflection fluctuations, as seen from the r_x in [μm] and r_y in [μm] measurement signals.

Figure 6 shows the time and frequency domain of a pressure transducer measuring the flow and according phenomena with their pressure pulsations acting on the rotating and stationary part of the machine unit. Figure 7 shows the resulting behavior of the turbine shaft at the rotating reference system. The next signal to consider is the turbine casing, as this sensor is applied at the absolute reference system and showcases the machine supporting system.

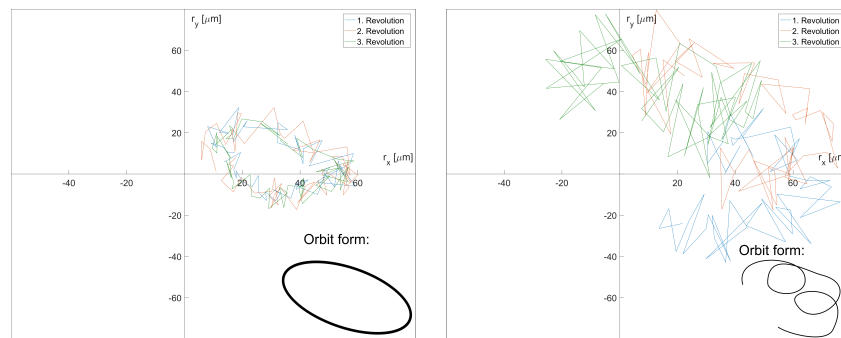


Figure 7. Turbine shaft orbits at best-efficiency point (BEP) (left) and part-load (PL) point (right).

The absolute turbine bearing vibration a_{THBy} shows a significant difference depending on the operating point. For example, in the part-load (PL) point, the vibration is more than three times higher compared to the best efficiency point, as shown in Figure 8.

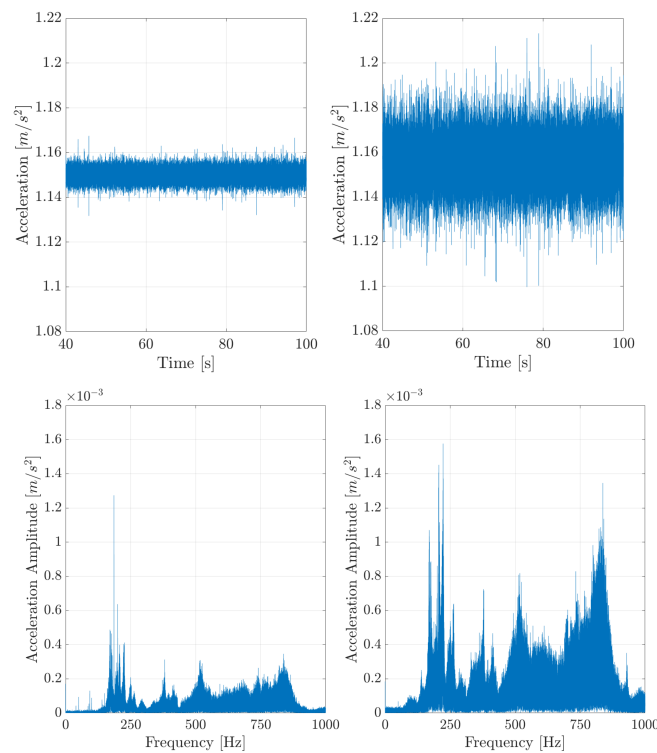


Figure 8. Acceleration sensor turbine bearing a_{THBy} in the time and frequency domain at best-efficiency point (BEP) (left) and part-load (PL) point (right).

Additionally, one can see the appearance of higher frequencies, whereas the expected lower DTV frequencies are missing. This leads to the conclusion that the DTV and resulting pressure fluctuations are detectable at those sensors directly attached to the fluid or rotating machine unit domain. Accordingly, the DTV does not affect the turbine bearing and subsequent attachment. At PL, we see frequencies in the 230–250 Hz range, which could originate from the VOS. Nevertheless, that has to be proofed separately and possibly detected by correlating other sensor signals.

Another interesting sensor that links the flow domain with the rotating part of the machine unit is the acceleration sensor a_{Hub} in $[m/s^2]$. That one is installed in the runner hub. This sensor provides acceleration values in the longitudinal axis of the turbine shaft and helps determine RSI, DTV, and VOS frequencies. Figure 9 shows a waterfall diagram of this sensor at all load levels and a frequency range of 0–500 Hz.

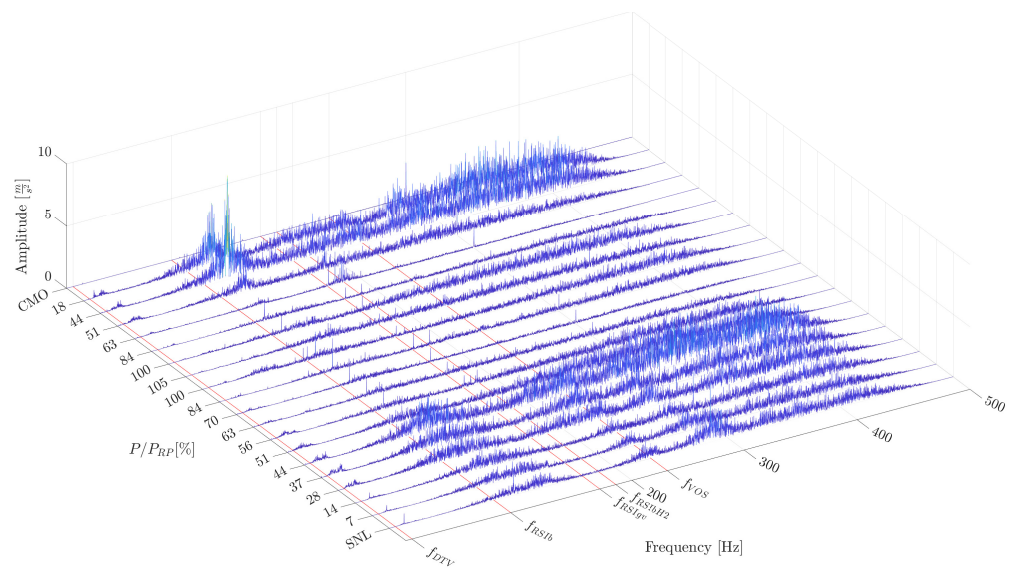


Figure 9. Waterfall diagram of a_{Hub} showing acceleration amplitudes in $[m/s^2]$ versus frequencies in $[Hz]$ versus load steps in $[\% P/P_{RP}]$.

The waterfall diagram shows some RSI frequencies, including harmonics. In addition, other frequency bands in the upper-frequency range are visible. The diagram also shows the load points where compressed air was injected into the machine. The PL points 63%, 51%, 44%, and 18% before the CMO are those operating points which, according to Figure 4, are in the range of compressed air injection. The injection is intended to stabilize the machine's behaviour and to prevent undesirable flow phenomena. However, one can see that in the range of approximately 125 Hz in the PL load points 44% and 18%, a flow phenomenon must be amplified because, at the same PL load points without compressed air injection, the amplitudes of this frequency band are much lower.

Table 2 summarizes the frequencies, according to FIGURE 8 of PART I [1], which have been detected from the prototype measurements.

Table 2. List of known frequencies and their harmonics, adapted from [31].

Phenomena	Frequency and Harmonics
Draft Tube Vortex (DTV)	1.4 Hz , 2.8 Hz, 3.2 Hz, 4.6 Hz, 6 Hz
Rotating Frequency	7.14 Hz, 14.28 Hz, 21.42 Hz, 28.56 Hz, 35.7 Hz, 42.84 Hz
Grid Frequency	50 Hz, 100 Hz, 150 Hz, 200 Hz, 250 Hz, 300 Hz, 600 Hz
Blade Passing Frequency (RSIb)	92 Hz, 185 Hz, 277 Hz
Guide Vane Passing Frequency (RSIgv)	171 Hz, 342 Hz, 513 Hz
Vortex Shedding (VOS)	232 Hz, 464 Hz, 696 Hz, 928 Hz

3.2. Correlation of Signals (Aspect 2)

As already mentioned in Section 2.2 and the description of Figure 9, compressed air was injected during the measurement from the overload range to the minimum load point. Looking at the part load range of 50–60% of the machine where stabilizing air was injected, the same performance fluctuations can be observed without compressed air (see Table 3, where P_{hydr} , P_{mech} , and P_{el} are correlated at different load steps and with/without air injection). This leads to the assumption that the injected air through the turbine cover does not sufficiently suppress the part load draft tube vortex rope in this particular case of machine design. This assumption is also confirmed by considering the Fast-Fourier-Transformations (FFT) in Table 3. A DTV frequency of 1.4–1.5 Hz was detected in both directions, the PL-up and PL-down load points. This frequency indicates the presence of

a DTV in this load region. This frequency was also observed in Figure 6. However, this frequency does not appear in the BEP, which is consistent with the theory. Surprisingly, the amplitude in the PL-down (with stabilizing air) is higher than in the PL-up (without stabilizing air), just as if injecting air would intensify this effect. Designs of other machine setups where the air injection is, for example, realized through the hub could lead to a different behavior. Thus, the position of air admission plays an important role in the calculation of the fatigue strength and the subsequent determination of the remaining lifetime of the runner. If the damaging loads do not decrease due to the admission of air, the runner will remain fatigued, which has far-reaching consequences in the assessment process.

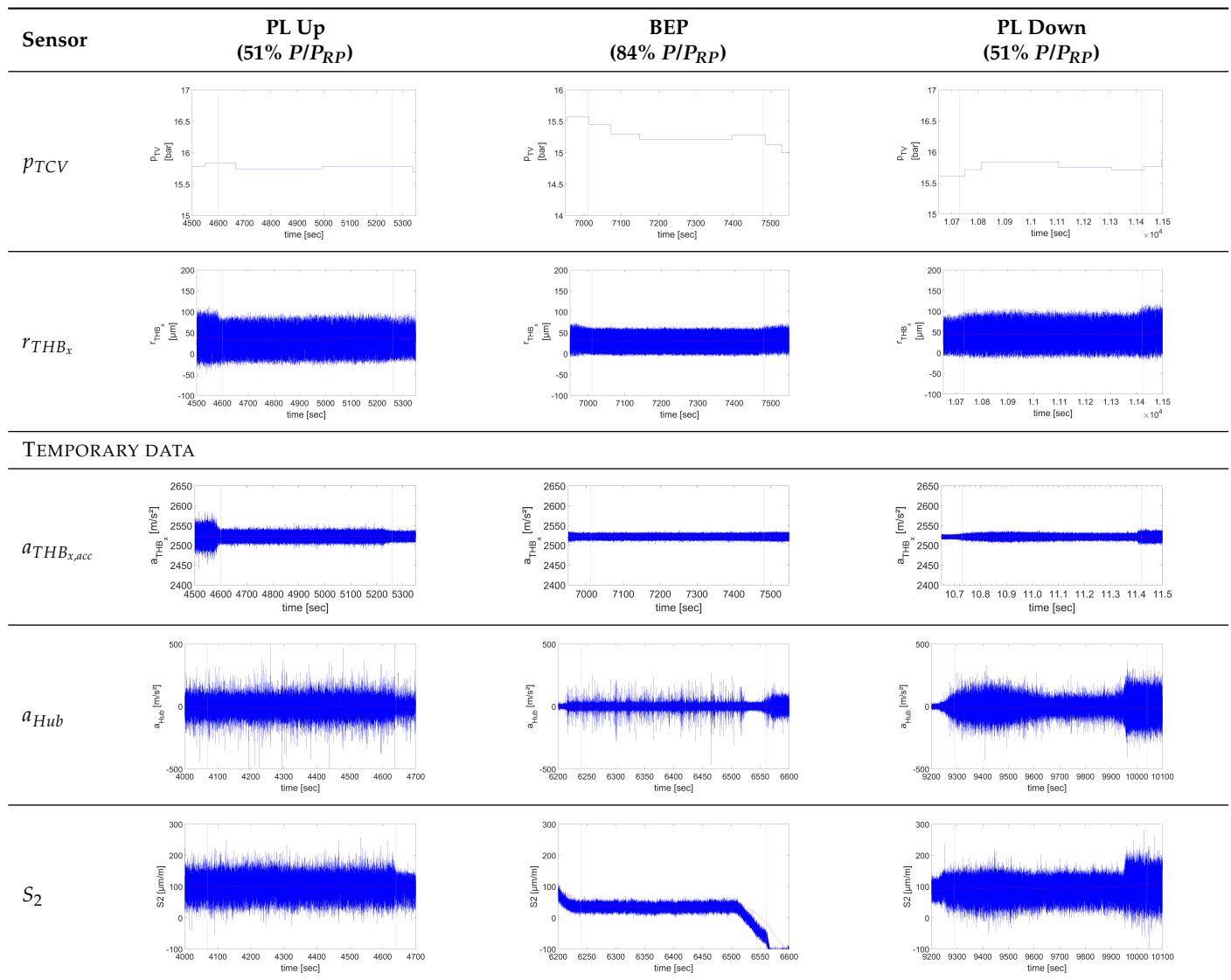
Since the air is injected through the turbine cover, a dynamic pressure sensor at this point would be an advantage. A time signal with higher resolution at this point of the machine would help to calibrate the numerical flow simulation more precisely in order to better understand the underlying two-phase flow phenomenon. In the future, an application of a dynamic pressure sensor at this point should be planned for new machine sets. The problem with existing machine sets is the difficulty of instrumentation due to space restrictions.

Table 3. Time and frequency domain of PL and BEP load steps, Up–without air injection, Down–with air injection.

Sensor	PL Up (51% P/P_{RP})	BEP (84% P/P_{RP})	PL Down (51% P/P_{RP})
POWER SIGNALS			
$P_{hydr}, P_{mech}, P_{el}$			
P_{mech}			

Based on the above findings, Table 4 compares representative measurement signals in order to understand the machine behavior at different operating points. The time signals of the PL points (51% P/P_{RP}) are compared with those at the BEP (84% P/P_{RP}), where the dynamic loads on the machine should be the lowest. The interpretation of the entire machine set can be conducted from two different points of view, namely the perspective of the absolute and relative system. In the absolute system, all components are subsumed that are stationary and not rotating, e.g., the bearing, the turbine cover or generator stator, while in the relative system, the rotating components, e.g., the runner, the shaft or the generator rotor are conducted. When correlating measurement signals, it will be important to distinguish whether the used sensors contribute to one or the other system. According to Table 4, the sensors for the signals r_{THB_x} , a_{Hub} , and S_2 are assigned to the relative system, while the remaining sensors for the signals p_{TCV} and $a_{THB_{x,acc}}$ contribute to the absolute system.

Table 4. Correlation of selected parameters.



Correlating now the time signals of Table 4, one can see on a first shoot that the part load operation (51% P/P_{RP}) is much more harmful than the operation at the best efficiency point (84% P/P_{RP}). This obvious fact gets best visible when looking at the accelerometers either at the hub a_{Hub} or at the bearing $a_{THB_{x,acc}}$. Both show higher amplitudes at the PL area than at the BEP point. The strain gauge S_2 shows the same tendency as well. The future question of evaluation is the degree of damage of all operational points to the overall lifetime assessment. Furthermore, the second step is to interpret the damage by investigating monitoring sensors that are permanently applied instead of temporary measurements. Therefore, this table was divided into measures for an absolute and relative system and permanently and temporarily installed sensors. At the temporary data, one can see tendencies, which indicate the effects of the rough part load operation compared to the best efficiency point. The same tendency shows the permanently installed sensor and both signals will be correlated in further publications to obtain the proper assessment model for the investigated part.

A brief example of such an investigation would be the question of air admission affecting the energy conversion and machine behavior. As already mentioned above, the injection position plays a big issue at the machine unit investigation. Comparing the time signals of 51% P/P_{RP} (PL up—without air) and 51% P/P_{RP} (PL down—with air),

one could detect the following: in the absolute reference system, the signal amplitude is reduced significantly, which can be observed at sensor $a_{THB_{x,acc}}$, whereas in the relative reference system, the attached sensors show the same behavior. A global interpretation of this correlation would lead to the resulting formulation—at the investigated machine setup, the injected air reduces the casing vibration of the turbine bearing, resulting in a longer lifetime, whereas the rotating parts see the same load and last shorter.

Suppose we correlate the number of recorded signals with the flow phenomena one wants to detect. In that case, we obtain a first matrix (see Table 5) that can be used for further considerations in machine diagnosis.

Table 5. Frequencies of DTV, speed, grid frequency, RSI and VOS, adapted from [31].

Phenomena	a_{THB_x}	a_{THB_y}	$a_{GV,1}$	$p_{con.1}$	$p_{con.3}$	a_{con}	DMS – D2	DMS – S2	a_{Hub}
Draft Tube Vortex (DTV)				X	X		X	X	X
Rotating Frequency	X	X		X	X		X	X	X
Grid Frequency	X	X		X	X				X
Blade Passing Frequency (RSIb)	X	X	X	X	X	X			X
Guide Vane Passing Frequency (RSIgv)	X	X	X	X	X	X	X	X	X
Vortex Shedding (VOS)	X	X	X	X	X	X			X
Sensor group	Perm. MD	Temporary Validation				Temporary Assessment			
MD syst. upgrade	o	o	++	+	+	++	--	--	--

o = neutral, as already installed, + = positive, ++ = extremely positive, -- = not suitable.

Table 5 contains sensors of the different groups from Table 1 and indicates which sensor can be used to detect flow phenomena. In addition, a classification has been made as to which sensor seems most suitable for a machine diagnostics upgrade. a_{THB_x} and a_{THB_y} are already installed in this hydropower plant and serve, therefore, as a base. Acceleration sensors $a_{GV,1}$ and a_{con} mounted outside of the machine have the highest potential to be included in a machine diagnosis setup. The installation is rather easy and the sensor lifetime is according to industrial standard. Pressure transducers such as $p_{con.1}$ and $p_{con.3}$ have a good potential from the data quality but lower opportunities to be included in a machine diagnosis system due to the sensor lifetime. Sensors such as DMS – D2, DMS – S2, or a_{Hub} deliver the most accurate data, but have a limited lifetime and are, therefore, not suitable to be included in a permanent machine diagnosis system.

3.3. Lifetime Determination by Using Strain Gauges

During the measurement, the stresses occurring at the strain gauge positions over the entire operating range of the system were recorded. Similar to what was already shown in PART II [2], the static and dynamic stress components, as well as the damage factors and the resulting values of the lifetime at the strain gauge positions, were evaluated using the measured stress signal. The methodology used for this has already been explained in detail in PART II [2]. Results for selected strain gauges and operating points can be seen in [30]. A description of the stress evaluation and corresponding procedure is already published in [30,32].

3.3.1. Stress Evaluation at the Position of Strain Gauges

Static Stress Results

Figures 10 and 11 show the static mean stress σ_m , defined as the arithmetic mean value of the measured signal at the suction and pressure side transitions from blade to hub and

shroud on the trailing edge. The results are normalized by the yield strength σ_y of the runner material X5CrNi14-3 received from a test report of the Fraunhofer Institute [33].

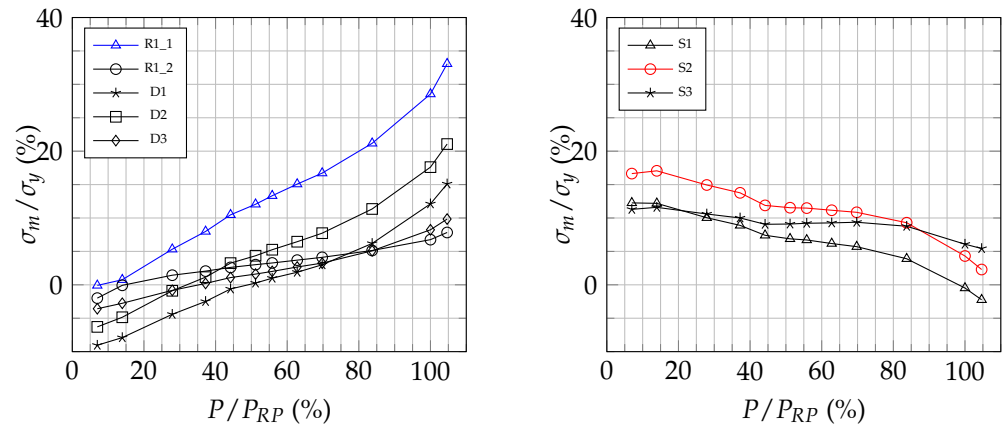


Figure 10. Static mean stresses at strain gauge positions close to the runner hub for PS (left) and SS (right).

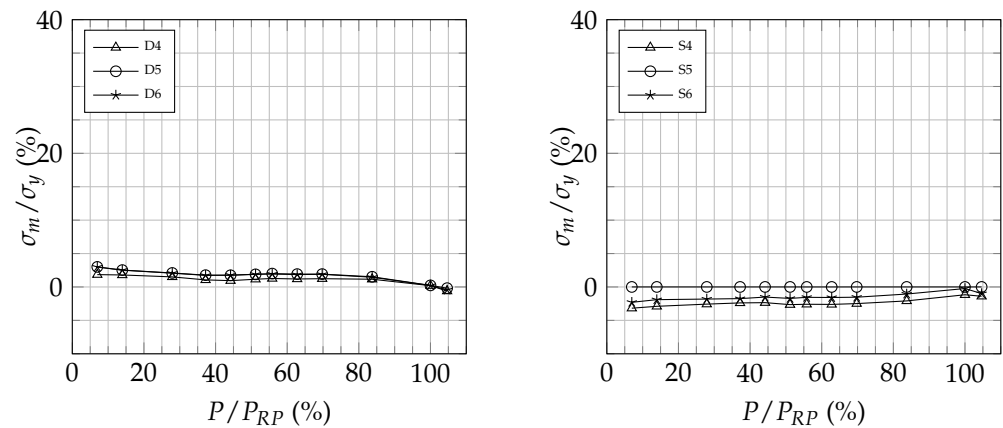


Figure 11. Static mean stresses at strain gauge positions close to the runner shroud for PS (left) and SS (right).

At the transition of the runner blade to the runner hub, significantly higher mean stresses occur on both the pressure and suction sides than at the shroud. This behavior is consistent with the numerical results from PART II [2] and has also been shown in earlier investigations of an impeller with similar specific speed n_q (see [1] for the definition of n_q). The absolute maximum results for the first principal stress of the rosette R1-1 at overload (105% P/P_{RP}), whereby even this value is still clearly below the failure-critical material parameters. Furthermore, it can be seen that with increasing power, the position of the highest measured static stress changes from the suction-side strain gauge S2 to the pressure-side placed rosette R1 in the range from (37–44% P/P_{RP}).

Dynamic Stress Results

To compare the dynamic stresses at different strain gauge positions throughout the whole operating range of the plant, the normalized dynamic stress values (σ_a/σ_y) of the measured time signals are shown in Figures 12 and 13.

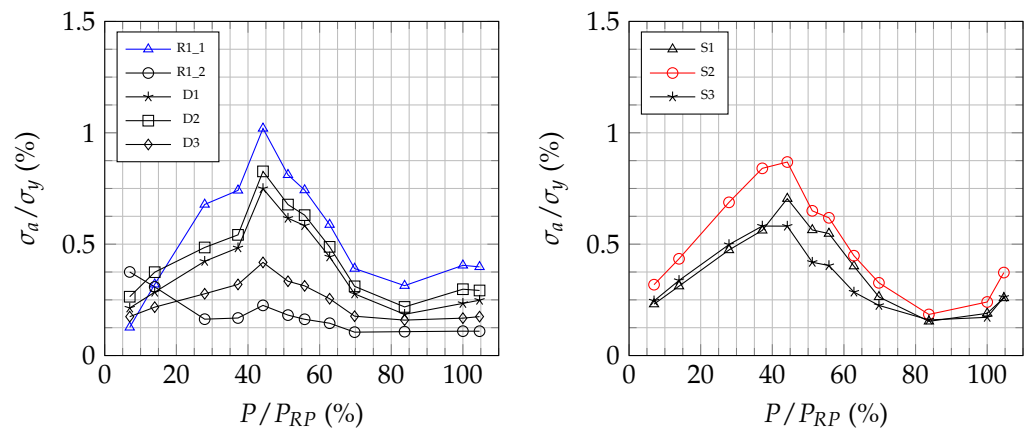


Figure 12. Dynamic stresses at strain gauge positions close to the runner hub for PS (left) and SS (right).

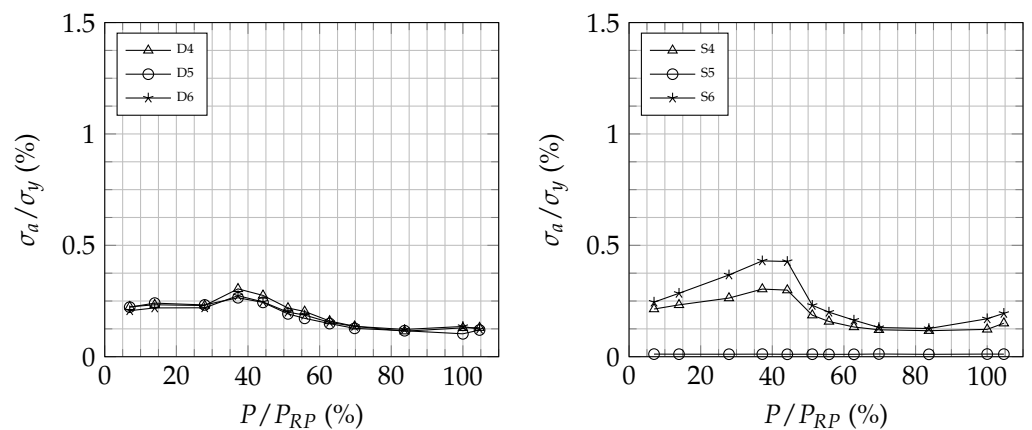


Figure 13. Dynamic stresses at strain gauge positions close to the runner shroud for PS (left) and SS (right).

As with the static stresses, the dynamic stress components are also significantly higher at the transition to the hub than at the shroud. The highest values are again found at the strain gauge positions R1 and S2 with the absolute maximum for R1 at (44% P / P_{RP}). In general, it is easy to see that the amplitudes near the RP and BEP are lower than at the remaining operating points. Towards lower power, there is a significant increase in dynamic stresses for all strain gauges with the maxima between (37–44% P / P_{RP}). At the deep part load, these effects then decrease again. This behavior indicates that partial load vortices occur in the range of (37–44% P / P_{RP}), which mainly attach themselves to the runner hub and cause increased dynamic stresses.

3.3.2. Stress Concentration Factor (k-Factor Concept)

Stress concentration factors are used to evaluate the maximum stress intensity points (hotspots) from a nominal stress point. The entire concept has already been discussed in SECTION 3.3.1 in PART I [1] and should not be repeated here. In summary, there are two challenges to cover: the shifting hotspot at each load step of the turbine and the unknown multiplication factor for the notch influence, as a Francis runner is no simple construction part. The consequence is that the k-factor concept is not applicable on this kind of construction.

3.3.3. Analytical Strength Assessment

According to [34], the analytical strength assessment can calculate the fatigue strength of simple or welded steel components. This analysis can either be performed with nominal

stresses using k-factors or local stresses. The problem of stress intensity factors has already been discussed above and in detail in SECTION 3.3.1 in PART I [1]. The present design of a Francis runner and the variability of the hotspot at different load steps make using k-factors "de facto" impossible. Therefore, it is necessary to use the method of local stresses in an analytical strength assessment according to [34]. However, a closer look at this alternative also shows that design factors are required to evaluate form factors and notches. The authors also believe this analysis is not target-oriented and can only be conducted with further stress calculations using FE methods.

Therefore, according to Figure 1, the new method was developed, and an analytical strength assessment according to [34] was omitted. The prototype measurements and evaluations of the signals serve to validate the simulation. Stress analyzes are only carried out at those points that can be unambiguously assigned and correspond precisely to the numerical simulation. They give a first impression of the existing mechanical stresses in the runner and serve as a basis for further correction factors derived from the difference between computation and experiment.

3.3.4. Damage Factors

The load spectrum obtained from the measured data by means of RFC is compared with the SN-curve of the runner material to determine the damage. As already described in PART II and applied in [30,32,35] and other publications, the modified damage hypothesis "Miner Elementar" according to Palmgren and Miner [36] is used. As can be seen from the static and dynamic stress evaluations, R1 and S2 are the failure-critical strain gauge positions. For this reason, the associated damage factors were determined only for these two strain gauges.

As Figure 14 shows, the damage level is decreasing towards the BEP and RP for both strain gauges. Except for (7% P/P_{RP}), the rosette R1 shows a lower damage factor. These results correspond to the behavior of the dynamic stresses shown in Figures 12 and 13, where the values are smallest at the same operating points. Going down further in part load, a continuous increase of the damage can be observed with the maximum value at (44% P/P_{RP}) for R1 and S2, where also the highest stress amplitudes occur. In deep part-load, the values are decreasing again.

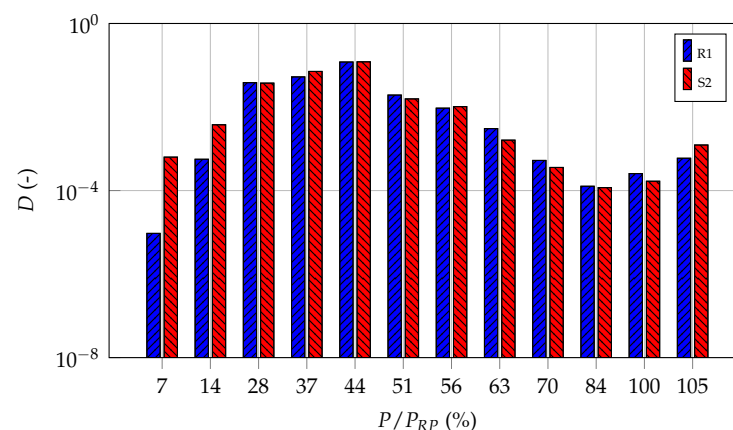


Figure 14. Damage factors at DMS R1 (left) and S2 (right) for 1 year of operating time.

3.3.5. Lifetime Prediction at the Position of Strain Gauges

However, in order to be able to make actual statements about the fatigue and further the lifetime of the Francis runner, the damage factors shown are not sufficient. The knowledge of a corresponding load spectrum of the plant is necessary. For this purpose, as already in PART II, the fictitious operating times of the two load scenarios base load and grid stabilization published in PART I [1] (see FIGURE 5, p. 7) were used. The values of the

service life determined from the measured stresses with the aid of the two load scenarios are shown in Table 6.

Table 6. Expected lifetime for R1 and S2 in years for base load and grid stabilization

Position	Base Load [Years]	Grid Stabilization [Years]
R1	2386.2	45
S2	2082.5	43.2

Although the damage factors in the partial load are slightly higher for R1, the position of the S2 strain gauge turns out to be critical for failure, as can be seen in Table 6, due to the weighting with the associated operating times for both scenarios. However, it should be noted that, especially for grid stabilization, there is only a small difference between the expected lifetime.

4. Discussion

Based on the above illustrations and results, the following points of discussion are of interest:

1. Looking at the individual flow phenomena and measurement signals, one can see the different applicability of individual sensors. There is a specific correlation between flow phenomena and sensor application. This point was illustrated in Section 3.1 for different load points. Accordingly, it should be taken into account when correlating sensors and data. The resulting frequencies have been summarized in Table 3.
2. An important result is Table 5. Within this table, one can see the possibility to detect a specific flow phenomena with different kinds of sensors. Furthermore, this table is just an excerpt of all possible sensors. The sampling rate and the sensor application location make this table so specific. This table has two particular advantages: on the one hand, the chance to add some additional sensors to the machine diagnosis system and, on the other hand, the availability to build a virtual/soft sensor detecting flow phenomena from a multi-sensor level.
3. The mechanical stresses to assess the lifetime of a Francis runner can only be determined at predefined points. Depending on the selection of the points to be examined on the runner and the number of available sampling channels on the data acquisition system, either linear strain gauges or strain gauge rosettes are used. Linear strain gauges have the advantage of occupying only one recording channel but must be attached at points where a uni-axial stress gradient is expected. This usually leads to measuring points further away from the hotspot, the point with the maximum mechanical stresses. However, several linear strain gauges are often applied at these points for redundancy reasons. Suppose the hotspots are already known from previous investigations. In that case, a strain gauge rosette consisting of three linear strain gauges at different angles to each other can be applied in this area. The informative value of the stress measurement increases considerably as long as the hotspot does not change under different load influences. A suitable selection of strain gauge measuring points requires a specific experience with the fatigue assessment of Francis runners. This inevitably leads to the discussion of extrapolation in the direction of those points with the highest mechanical stresses, which are decisive for the fatigue strength calculation. In many technical applications, the influence of possible geometric changes, such as notches, curves, and cross-section changes, is considered in this context by introducing stress concentration factors, so-called k-factors. Since the dynamic loads are used as the design basis for the fatigue strength calculation, and these can change locally from load case to load case, the k-factors would also have to be adjusted in each calculation step to make statements that are true to reality. This is not feasible with a purely metrological approach. As a solution, either static k-factors are chosen,

which can significantly distort the result, or a combination with strength calculations is carried out.

Since the locations with the maximum mechanical stresses depend on different load cases and the underlying flow phenomena, a combination of experiment and simulation is the best possible solution. Only in this way can moving hotspots be assessed more accurately and the fatigue strength calculation improved. The result is a validation system that supports measurement and numerical calculation.

5. Conclusions

The following conclusions could be drawn:

+ Additional sensors:

In the section at the vaneless space, an unsteady pressure measurement sensor would be very useful to detect pressure fluctuations, but the instrumentation is very difficult in this region and requires in existing machines a major effort if a monitoring point does not already exist. A time signal with a higher resolution at this point of the machine would help to calibrate the numerical flow simulation more precisely in order to better understand the underlying two-phase flow phenomenon.

The main part of the installed pressure gauges are chiefly used for steady static pressure measurements. For many applications, it is very important to know the pressure distribution from the inlet to the outlet of the machine. Afterward, all steady static pressure monitoring points are listed and described, starting from the turbine closing valve and then in flow direction through the machine, ending at the draft tube outlet, as shown in Figure 2.

In the future, an application of a dynamic pressure sensor at this point should be planned for new machine sets. The problem regarding existing machine sets is the difficulty of instrumentation due to space restrictions.

+ K-factor concept versus local mechanical stresses:

The main point is that one cannot investigate the hotspots with measurements. Significantly, if the hotspots vary, meaningful measurements are not possible. Such investigations are performed because stresses are measured at the points where known conditions are expected; moreover, an extrapolation takes part.

+ Need for numerical calculation with validation through measurements:

Taking previous conclusions into account, the way to perform better and newer fatigue evaluations is a combination between numerical simulations and measurements. Numerical simulations can give us a better insight according to the maximum stresses but should be validated by precise measurements.

+ Virtual/soft sensor:

The current results conclude the possibility of developing a virtual/soft sensor. This combines several physical sensors to detect certain flow phenomena better and limit them in the characteristic operating field. This topic will be displayed in Part IV of this paper series.

Author Contributions: Conceptualization, E.D.; methodology, E.D., A.M. and J.U.; validation, S.S., M.M., F.H. and A.M.; formal analysis, E.D.; investigation, S.S., A.M., J.U. and E.D.; data curation, S.S., M.M. and F.H.; writing—original draft preparation, E.D., S.S., J.U. and F.H.; writing—review and editing, F.H., C.B., A.M. and J.U.; visualization, S.S., M.M. and F.H.; supervision, E.D. and A.M.; project administration, E.D.; funding acquisition, E.D. All authors have read and agreed to the published version of the manuscript.

Funding: Open Access Funding by TU Wien. The MDREST project was funded by the FFG—Austrian Research Promotion Agency (BRIDGE, No.861560) and the associated research partners Brüel & Kjaer Vibro GmbH and Voralberger Illwerke AG. The DIGI-HYDRO-project is funded by the Austrian Climate and Energy Fund (No.881188) and is carried out within the framework of the Energy Research Programme 2019. Associated research partners are HAKOM Time Series GmbH, VibroConcept GmbH, and VRVis Zentrum für Virtual Reality und Visualisierung Forschungs-GmbH.

Data Availability Statement: No public data available.

Acknowledgments: The authors would like to thank the project partners Brüel & Kjær Vibro GmbH and Voralberger Illwerke AG for their contribution in the course of the research project MDREST. The authors would like to thank the project partners HAKOM Time Series GmbH, VibroConcept GmbH, and VRVis Zentrum für Virtual Reality und Visualisierung Forschungs-GmbH for their contribution in the course of the research project DIGI-HYDRO. The computational results presented have been carried out by using the Vienna Scientific Cluster (VSC3 & VSC4). The authors acknowledge the TU Wien University Library for financial support through its Open Access Funding Program.

Conflicts of Interest: The authors declare no conflict of interest.

Abbreviations

The following abbreviations are used in this manuscript:

BEP	Best Efficiency Point
CFD	Computational Fluid Dynamics
CMO	Condenser Mode
DT	Draft Tube
DTV	Draft Tube Vortex
FE	Finite Element
FEA	Finite Element Analysis
FFT	Fast-Fourier Transformation
FSI	Fluid Structure Interaction
FSO	Free Surface Oscillation
H_{netto}	Net head
ICV	Inter Blade Cavitation Vortex
LGB	Lower Generator Bearing
MATLAB	Mathematical software tool
PL	Part-Load
RFC	Rainflow Counting
RSI	Rotor–Stator Interaction
SCADA	Supervisory Control and Data Acquisition
SNL	Speed-No-Load
SPP	Stochastic-Pressure Pulsation Cavitation
THB	Turbine Bearing
TSM	Time Series Management
UGB	Upper Generator Bearing
VISPLORE	Trade name of VRVis Software
VOS	Vortex Shedding

Appendix A. Sensor Application and Characteristics

The Appendix contains the list of measurement signals and their usage. In some cases, measurement signals contain more than one single signal. In that case, the measurement signal is dedicated to the position of the sensor.

Appendix A.1. Permanent Installed Sensors to Acquire Operational Data

These sensors are installed by the operator in order to generate appropriate data for the operation management. The following operating parameters were used for the evaluation method to allow a correct determination:

1. **Head Water level** z_{HW} in (m);
2. **Tail Water level** z_{TW} in (m);
3. **Guide vane opening** a_0 in (%);
4. **Turbine discharge** Q in (m^3/s);
5. **Turbine Closing Valve pressure** p_{TCV} in (bar);
6. **Spiral Case pressure** p_{SC} in (bar);
7. **Runner Inlet or Vaneless Space pressure** p_{RN} in (bar);

8. **Turbine Cover pressure** p_{CO} in (bar);
9. **Draft Tube Cone pressure** $p_{con.2}$ in (bar);
10. **Speed** n in (min^{-1});
11. **Electrical Power** P_{el} in (MW).

Further descriptions and sensor characteristics are presented in the following subsections.

Appendix A.1.1. Water Levels (z_{HW} , z_{TW}) and Guide Vane Opening A_0

Regarding operational or global parameters, head- and tail-water level as well as the guide vane opening have been measured. Thereby, the net head can be calculated and the operation point of the turbine in the hill chart can be evaluated. Depending on the design and environment of the plant as well as operating conditions, huge shifts in terms of head-water and/or tail-water during energy supply are possible. The measurements are performed by the use of static pressure sensors which are determined by the derivation from the base water level. The guide vane opening a_0 determines the discharge. It is measured by evaluating the movement of the hydraulic cylinder, which is used to adjust the guide vane position. The global parameters are provided by the operator.

Appendix A.1.2. Turbine Discharge Q

Discharge measurements are generally a crucial task at hydropower plants, and therefore, tasks of high interest including matters of accuracy. As many parts are encased in concrete for stability reason, the application of ultrasonic devices is not always possible. Therefore, other discharge measurement methods have to be used, such as pressure–time methods or dynamic pressure probes. The turbine discharge Q is regulated by the guide vane opening and defines the machine operation point. In the case of the investigated hydropower plant II of the research project, it was measured by using the Winter–Kennedy method, which is a relative discharge measurement. In contrast to ultrasonic measurement, no inlet and outlet run is needed and the response time is shorter. The turbine discharge Q is usually well represented by:

$$Q = \Delta p^n k \quad (\text{A1})$$

with the pressure difference Δp between the inner and outer tap, n , theoretically equal to 0.5 (see [37]) and the factor k . The pressure taps are located at the spiral case and arranged according to IEC 60041 [37]. The inner and outer pressure taps and a drawing of the principal arrangement as defined by IEC 60041 are shown in Figure A1. The gauge is permanently installed and the signal is taken from the power plant monitoring system.

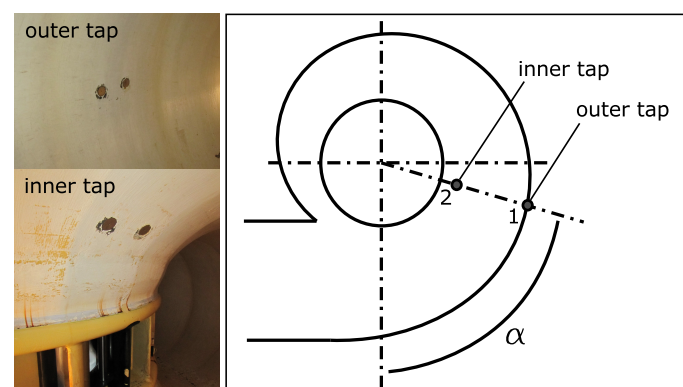


Figure A1. Schema according to IEC 60041 [37] and pressure tabs for the Winter–Kennedy measurement, where $\alpha = 45$ to 135 .

Main technical data of the equipped sensor are listed in Table A1 and the signal is sampled with 10 Hz.

Table A1. Main characteristics of the pressure transducers Δp .

Characteristic		Value
Measurement range	bar	0 ... 10
Resolution	bar	0.02
Measurement accuracy	%FSO	+/-0.25

The main part of the installed pressure gauges are chiefly used for steady static pressure measurements giving a RMS value at the capturing point. Afterwards, most of the steady static pressure monitoring points are listed and described in flow direction through the machine, starting from turbine closing valve and ending at the draft tube outlet as shown in Figure 2.

Appendix A.1.3. Turbine Closing Valve p_{TCV} , Spiral Case Entry p_{SC} , Runner Inlet or Vaneless Space p_{RN}

The first three measuring points are permanently installed monitoring points. p_{TCV} is situated at the penstock in front of the turbine closing valve and the measurement section p_{SC} after the valve at the spiral case inlet. p_{RN} is located between the guide vanes and the runner at the so-called vaneless space. The main characteristics of the pressure gauges can be found in Table A2. The sensor type is the same for all three measuring points and the signal is sampled at 10 Hz. The permanent installation of the pressure sensor p_{SC} behind the turbine closing valve and at the beginning of the spiral case is shown in Figure A2 and a detailed view is given in Figure A3.

**Figure A2.** Position of the spiral case pressure sensor.**Figure A3.** Details of the permanent installation.

Table A2. Main characteristics of the pressure transducers p_{TCV} , p_{SC} , and p_{RN} .

Characteristic		Value
Measurement range	bar	0 ... 25
Resolution	bar	0.05
Measurement accuracy	%FSO	+/-0.25

Appendix A.1.4. Turbine Cover p_{CO} and Draft Tube Cone $P_{Con.2}$

The monitoring point p_{CO} is placed at the turbine cover after the labyrinth sealing. This allows a lower measuring range of 10 bar to be chosen. The gauge is also permanently installed. This value is important as a boundary condition for finite element simulations and for investigations regarding the leakage flow. The same pressure sensor is installed at the draft tube cone. The level of $p_{con.2}$ is $0.7 \cdot D_2$ below the runner outlet section. The sample rate of both sensors is 10 Hz and the important technical data are listed in Table A3.

Table A3. Main characteristics of the pressure transducers p_{CO} , $p_{con.2}$.

Characteristic		Value
Measurement range	bar	0 ... 10
Resolution	bar	0.02
Measurement accuracy	%FSO	+/-0.25

Appendix A.1.5. Speed N and Electrical Power P_{el} Measurement

The already-installed machine diagnosis set has a speed measurement included. This sensor and the respective value were used for validation of the other one. Figure A4 shows the permanent installation of the speed sensor, which is located beneath the lower generator bearing.

**Figure A4.** Regular speed sensor.

To complete the dataset for a unit assessment by using permanent installed sensors to acquire operational data, the electrical active power was taken from the machine diagnosis system provided by the power producer. Together with the mechanical power, the efficiency measures could be split up into a hydraulic and an electrical part. The sensor for the active power measurement is located at the generator side.

Appendix A.2. Permanent Machine Diagnosis Sensors

The permanently installed machine monitoring and diagnostic system primarily uses shaft vibration sensors, as listed in Table A4. Inductive vibration displacement sensors are used for relative shaft vibration measurement and vibration velocity or vibration

acceleration sensors for absolute casing vibrations. Axial vibration displacement sensors are extremely interesting for assessing axial machine motion but are rarely installed because this is very complicated when the machine is retrofitted. The combination of relative and absolute sensors enables the safe operation of the machine unit.

Table A4. Monitoring points—absolute bearing and relative shaft vibration.

Absolute Bearing Vibration			Relative Shaft Vibration		
Upper gen. bearing (velocity x)	a_{UGB_x}	mm/s	Upper gen. bearing (displacement x)	r_{UGB_x}	μm
Upper gen. bearing (velocity y)	a_{UGB_y}	mm/s	Upper gen. bearing (displacement y)	r_{UGB_y}	μm
			Upper gen. bearing (displacement z)	r_{UGB_z}	μm
Lower gen. bearing (velocity x)	a_{LGB_x}	mm/s	Lower gen. bearing (displacement x)	r_{LGB_x}	μm
Lower gen. bearing (velocity y)	a_{LGB_y}	mm/s	Lower gen. bearing (displacement y)	r_{LGB_y}	μm
Turb. bearing (velocity x)	a_{THB_x}	mm/s	Turb. bearing (displacement x)	r_{THB_x}	μm
Turb. bearing (velocity y)	a_{THB_y}	mm/s	Turb. bearing (displacement y)	r_{THB_y}	μm

Appendix A.2.1. Relative Shaft Vibration Measurements

Relative shaft vibration monitoring is essential for the orderly operation of the rotating part of the machine unit. Normally, non-contacting displacement sensors are used to determine the values of S_{max} or $S_{(p-p)_{max}}$ corresponding to the speed. Therefore, an additional speed measurement is mandatory. The normally permanent installation for this type includes two sensors with a 90° offset. By using this method, the relative movement of the shaft in relation to the fixed bearing casing serves as a control parameter for any further monitoring assessment. To complete the machine monitoring assessment, additional absolute bearing vibration sensors are installed. These sensors work on a velocity or acceleration measurement basis depending on the expected frequencies. Table A4 shows the position and installed equipment at the investigated machine unit. All shown sensor positions are installed permanently within the scope of the machine diagnosis program.

The permanently installed non-contacting displacement sensors which were used for this investigation work on an eddy-current principle and need, as a prerequisite, a metallic measuring surface, preferably made of 42CrMo4. The output voltage of the sensor is proportional to the distance between the probe tip and the measuring surface, within the displacement measuring range. Attention has to be paid to surrounding electromagnetic fields as these can falsify the measurements. Table A5 shows the main characteristic of these sensors. Installation and isolation of the cables have been implemented by the supplying company.

The used velocity sensors work according to the electro-dynamic principle and are used in order to detect the absolute bearing vibration of bearing cases. Installation of the sensors based on the specifications of the supplying company. Isolation has been verified and cables lead to the machine unit acquisition port. Table A6 shows, in brief, the main specifications of the used sensors.

Figure A5 shows the typical installation of x-y displacement measurement at the turbine guide bearing with non-contacting displacement sensors. The right part of the picture shows in detail the permanent installation of one sensor.

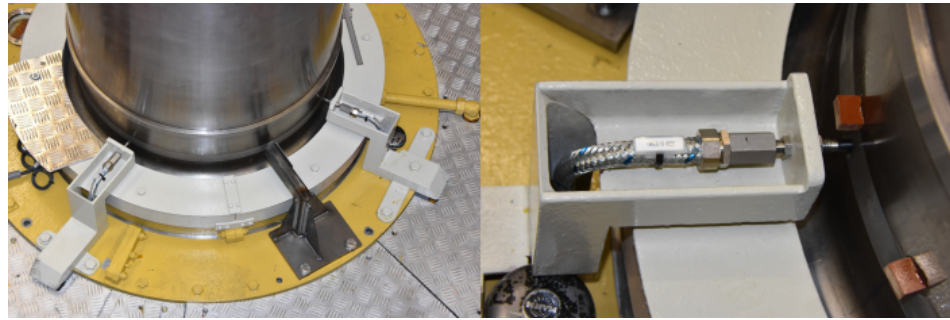


Figure A5. Non-contacting displacement sensors at the turbine bearing arranged in an angle of 90°.

Table A5. Main characteristics of the non-contacting displacement sensor.

Characteristic		Value
Measurement range	mm	1.5
Operating frequency range	kHz	0 ... 2.6
Sensitivity	mV/ μ m	8
Sensitivity error (at 22 °C)	%	< \pm 5
Deviation from ref. (at 22 °C)	%	< \pm 2

Appendix A.2.2. Absolute Bearing Vibration Measurements

Absolute casing vibration sensors measure the movements of the bearing casing, and thus, provide the basis for a complete vibration assessment of the shaft including the bearing. The casing movements must then be subtracted from the relative shaft vibrations to obtain an accurate measurement result concerning the shaft movement. Table A6 shows the characteristics of the installed sensors

Table A6. Main characteristics of the vibration velocity sensor.

Characteristic		Value
Measurement range		\pm 0.45 mm
Sensitivity	mV/mm/s	100
Sensitivity error (at 22 °C)		\pm 5%
Operating frequency range	kHz	0.01–2
Transverse sensitivity	%	<7
Resonance frequency	Hz	8

Appendix A.3. Temporary Measurements For Component Assessment

This area includes temporarily installed sensors because they cannot withstand the flow rate. These cannot be converted to permanent sensors. In our case, strain gauges and an accelerometer were installed.

The following operating parameters were used for the evaluation method to allow a correct determination:

1. **Strain gauges** D1 to S6 in (μ m/m);
2. **Hub vibration** a_{Hub} in (m/s^2).

Appendix A.3.1. Strain Gauge Measurements

In order to evaluate static and dynamic stress in the runner, strain gauges are used. Based on experience of the previous *GSG-GreenStorageGrid* project (funded in the framework of COMET—Competence Centers for Excellent Technologies by the Federal Ministry of Transport, Innovation and Technology, the Federal Ministry of Science, Research and Economy, the Vienna Business Agency, the Federal Province of Lower Austria and by the Federal Province of Upper Austria), 12 uni-axial strain gauges were installed at the trailing edge of one runner blade. The exact position was determined by the use of the finite

element method in combination with CFD analysis. Thereby, a stress maximum appears in the notch of the blade where the strain will not be uni-axial and can be considered as multi-axial. Therefore, besides linear strain gauges on the suction (S) and on the pressure side (D), a rosette (R1) was placed in the notch near the hub. Figure A6 shows the suction side of the runner blade as well as the locations of the strain gauges. The sensors D1/S1 and D2/S2 were installed close to each other in the flow direction to establish redundancy.

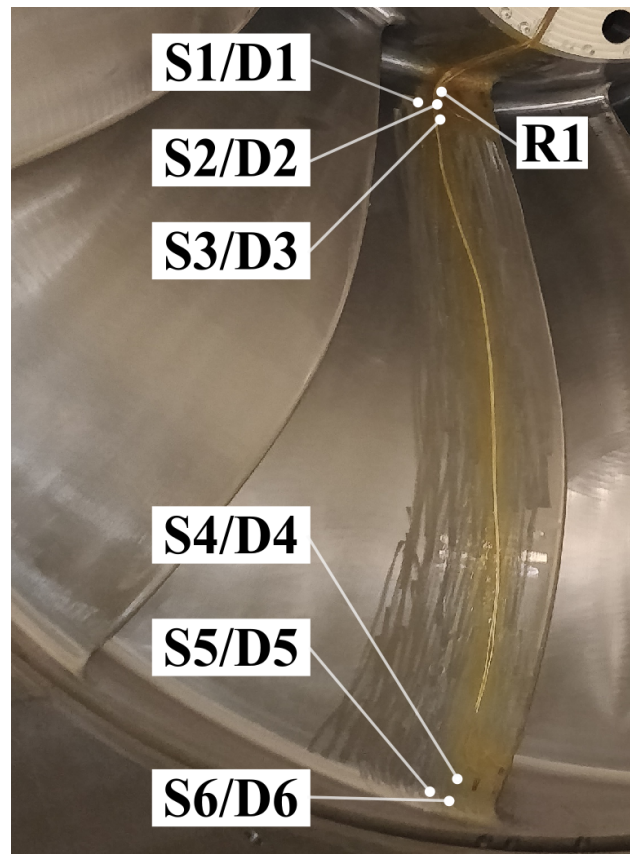


Figure A6. Strain gauge installation.

The main characteristic of the used strain gauges (linear and rosette) are shown in Tables A7 and A8. To cover the strain gauges and the attached cables, a material based on epoxy, acrylic, and polyurethane adhesives was used.

Due to the design of the machine set, data transmission through air by the use of a telemetry system was impossible. A data transmission through water would have been possible but much more complicated than a data-logger solution with the only problem being the installation of the casing in the hollow hub of the runner. Therefore, a cover adjusted to the hub geometry as shown in Figure A7 was designed. The cover was braced with the runner by four wedges and also a clamping beam further above in the hollow. All cables from the strain gauges were routed to the data-logger casing and attached to the acquisition unit with an electricity supply by corresponding batteries. Within the massive data-logger casing, there was also sufficient space to install an acceleration sensor to measure the values at this position.

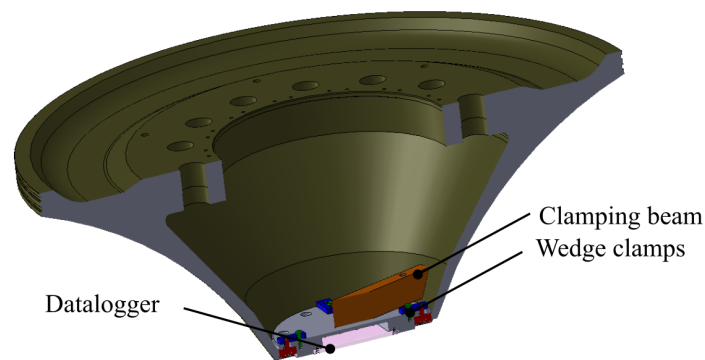


Figure A7. Sketch of the data-logger installation.

Table A7. Main characteristics of the linear strain gauges.

Characteristic		Value
Resistance	Ω	$350 \pm 0.35\%$
Gauge factor		$2 \pm 1.00\%$
Transverse sensitivity		-0.8%
Temperature factor of the gage factor		$93 \pm 10 [10^{-6}/K]$

Table A8. Main characteristics of the rosette strain gauges.

Characteristic		Value
Resistance	Ω	$350 \pm 0.50\%$
Gauge factor in direction a		$2.04 \pm 1.00\%$
Gauge factor in direction b		$2.04 \pm 1.00\%$
Gauge factor in direction c		$2.06 \pm 1.00\%$
Transverse sensitivity in direction a		0.4%
Transverse sensitivity in direction a		0.0%
Transverse sensitivity in direction a		0.0%
Temperature factor of the gage factor		$93 \pm 10 [10^{-6}/K]$

Appendix A.3.2. Hub Vibration Measurement a_{Hub}

One capacitive acceleration sensor with a measurement range of 10 g is mounted within the cover of the hollow hub to detect axial vibrations of the Francis runner. The arrangement of the sensor is pointed out in Figure 2 and the main technical data are listed in Table A9. The sample rate is 2 kHz, and similar to the strain gauges, the sensor is connected with the data logger in the rotating system.

Table A9. Main characteristics of the hub acceleration sensor a_{Hub} .

Characteristic		Value
Measurement range	g	$+/-10$
Sensitivity	mV/g	400
Bias calibration error	% of span	1
Non-Linearity	% of span	0.15

Appendix A.4. Temporary Validation Sensors

This group includes additionally installed sensors that have the potential to be included in the group of permanently installed sensors if it is determined that they have a positive impact on the evaluation. The following operating parameters were used for the evaluation method to enable a correct determination:

1. **Draft Tube End pressure** p_{DT} in (bar);

2. **Draft Tube Cone pressure** $p_{con.1}$ and $p_{con.3}$ in (bar);
3. **Turbine leakage water discharge** q^l in (l/s);
4. **Draft Tube Cone acceleration** a_{con} in (m/s^2);
5. **Cavitation measurements** a_{CV} in (m/s^2);
6. **Absolute bearing vibration** $a_{THB_{x,y}}$ in (m/s^2);
7. **Shaft Torque** T in (Nm);
8. **Speed** n in (min^{-1});
9. **Mechanical Power** P_{mech} in (MW).

Appendix A.4.1. Pressure Measurement

In the following section, the installed sensors are divided into two classes—gauges for steady and gauges for unsteady static pressure measurement. The fast response pressure transducers for unsteady measurement provide a time-resolved signal and the steady measurement gives a RMS value of pressure at the monitoring point.

Steady Static Pressure Measurements

In this section, additional temporary pressure measurement equipment for validation purposes has been installed. The end of the draft tube is especially of high importance in terms of boundary condition validation for CFD simulations. Most of the time, there is no permanent pressure measurement equipment at this cross section installed as the tail water level is of higher importance for the operator. At this measurement campaign, the existing pressure taps have been equipped with related transducers, and as the pressure fluctuations at this section are relatively low, normal steady static equipment with a lower sampling rate is used.

- **Draft tube outlet p_{DT}**
At the draft tube outlet section pressure transducers are additionally installed. The pressure taps are shown in Figure A8, in total there are two pressure taps on each side wall and two taps at the top. The main data of the sensor can be found in Table A10. It is a relative pressure transmitter with a metallic diaphragm and the sample rate is 100Hz.



Figure A8. Position static pressure measurement taps at the end of the draft tube p_{DT} .

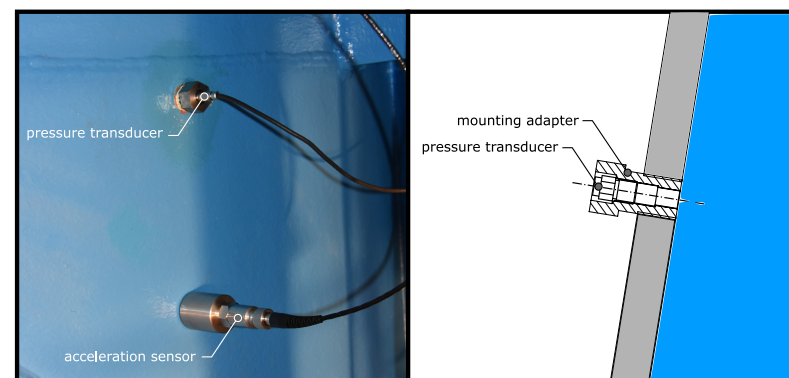
Table A10. Main characteristics of the pressure transducer p_{DT} .

Characteristic		Value
Measurement range	bar	0 ... 4
Measurement accuracy	%FSO	+/-0.2

Unsteady Static Pressure Measurements

To record the pressure fluctuations in the draft tube cone caused by the previously described flow phenomena, two piezoresistive absolute pressure transducers are installed.

- Draft tube cone $p_{con.1}$ and $p_{con.3}$
In contrast to piezoelectric transducers, these sensors are able to measure the static pressure as well as high-frequency pressure variations. Figure A9 shows the application of the utilized pressure sensor. The level of measurement point $p_{con.1}$ is $0.4 \cdot D_2$ below the runner outlet section and the second piezoresistive pressure transducer $p_{con.3}$ is mounted with a distance of $0.9 \cdot D_2$ to the runner outlet section with the diameter D_2 . To prevent disturbances, both sensors are front-flush mounted in the draft tube cone by using an adapter. The pressure is detected by a silicon measuring cell. It contains of a micro mechanical structure with piezoresistive resistors, which are implemented in a Wheatstone bridge. The important technical data are listed in the following Table A11 and the used sample rate is 2 kHz.

**Figure A9.** Position pressure transducer and acceleration sensor.**Table A11.** Main characteristics of the piezoresistive pressure transducer.

Characteristic		Value
Measurement range	bar	0 ... 10
Nominal sensitivity	mV/bar/mA	12.5
Maximum measurement uncertainty	%FSO	+/-0.2
Acceleration sensitivity	mbar/g	<0.3
Frequency response		
−5%	kHz	0 ... 19
−3 dB	kHz	0 ... 40

Appendix A.4.2. Turbine Leakage Water Discharge

The leakage water of the turbine is collected at three points on the turbine cover by a pipe system. The pipes lead to one pipe with a nominal diameter $DN = 200$ mm. All leakage water flows through this pipe into the draft. The pipes at the turbine cover are poorly accessible, very branched, and have no straight lined part of sufficient length to provide good flow conditions for discharge measurement. The collector pipe is encased in concrete and goes straight in one line from the turbine level down to the draft tube. It is, therefore, impossible to use clamp-on ultra sonic sensors. The problem was solved by using a flange as an access point for a dynamic pressure probe. It is basically a Prandtl

probe, picking up the total pressure p_{tot} and the static pressure p_{stat} . In effect, the dynamic pressure p_{dyn} is detected by a differential pressure sensor and the flow velocity v' can be calculated by:

$$v' = \sqrt{\frac{2}{\rho}(p_{tot} - p_{stat})} \quad (A2)$$

with the water density ρ . The inlet and outlet run is greater than $10 \cdot DN$, and therefore, the flow conditions at the probe should be satisfying. Assuming a distinctive fluid flow distribution, the discharge q' can be collected.

The flange, used as an access point, and a part of the dynamic pressure probe with the pressure connection points are shown in Figure A10. The main characteristics of the sensor are listed in Table A12.



Figure A10. Leakage water—access point and dynamic pressure probe.

Table A12. Main characteristics of the differential pressure transducer p_{dyn} .

Characteristic		Value
Measurement range	mbar	0 ... 100
Measurement accuracy	%FSO	+/-0.17

Appendix A.4.3. Draft Tube Vibration Measurements A_{Con}

The goal of this monitoring point is to detect specific vibration changes caused by different operation conditions and to record typical frequencies of different flow phenomena. An acceleration sensor with constant current power is mounted at the draft tube cone with a distance of $0.5 \cdot D_2$ to the turbine runner outlet section with the diameter D_2 . It is located between the two piezoresistive absolute pressure transducers—as shown in Figure A9. The acceleration sensor is developed and mainly used for measurement of vibrations at rotating machines such as turbines or pumps and works on the piezoelectric compression principle. The technical data are listed in Table A13.

Table A13. Main characteristics of the acceleration sensor a_{con} , $a_{THB_{x,y}}$.

Characteristic		Value
Measurement range	g	+/- 80
	Hz	4 ... 10k
Sensitivity (at 80 Hz, 23°)	mV/g	100
	mV/m/s ²	10.2
Transverse sensitivity (80 Hz)	%	<10
Accuracy of sensitivity	%	+/-5
Resonance frequency	kHz	35 +/-3

Appendix A.4.4. Cavitation Measurements

As previously discussed, there are several cavitation phenomena which may occur in a Francis turbine. As regards leading edge separation, i.e., cloud or bubble cavitation, the detection possibilities are rather rare. The usage of high-resolution accelerometers for the detection of the subsequent pressure pulsations due to bubble cavitation has been verified by laboratory tests [38]. In addition, prototype measurements have been performed to identify the best place for the mounting of these sensors, which is the end of the guide vane shaft. Pressure pulsations from the leading edge of the runner propagate against the guide vanes and the spiral case. At the investigated power plant, tests have been performed to measure the signal strength at the end of the guide vane, which has been excited by the pressure pulsations resulting from cavitation. The only challenge is the position at the guide vane end itself for acquiring a good and reliable signal. Another important point is the isolation of the sensors, as they are vulnerable to electric fields. This circumstances have been detected already at the laboratory tests and could be avoided by installing an isolation disk out of ceramic. Two different sensors have been tested at this measurement procedure to show both capabilities for future installations.

- Acceleration sensor a_{GV} .
Previous investigations [38] on the possibility of using piezoelectric compression accelerometers for cavitation measurements have shown that a high-resolution sensor is needed to record frequencies due to bubble cavitation. The used sensor is able to withstand very high-level, continuous vibrations and mechanical shocks up to 150 kms^{-2} and 1000 kms^{-2} , respectively. It has a sturdy construction and contains a PZ 45 piezoelectric element. This element is a ferroelectric ceramic that is prepared and treated to withstand very high dynamic stress with negligible zero shift problems. The housing material is stainless steel. Table A14 shows the main characteristics of the used sensor.

Figure A11 shows the installation of the acceleration sensor at the end of the guide vane with the support and ceramic isolation disc.

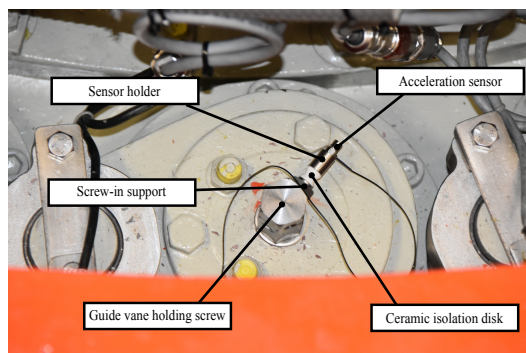


Figure A11. Position of the acceleration sensor for cavitation measurement.

Table A14. Main characteristics of the acceleration sensor a_{GV} .

Characteristic		Value
Measurement range	kHz	1 ... 54
Sensitivity	mV/g	0.19
	mV/m/s ²	0.0194
Accuracy of sensitivity	%FSO	+/-5
Transverse sensitivity	%	2.8
Mounted resonance frequency	kHz	180
Transverse resonance frequency	kHz	28

- Alternative stress energy transmitter a_{GV}
As a second possibility, a stress energy transmitter has been installed at the same

position as the acceleration sensor. Both signals could be compared for validation. Table A15 shows the main characteristics of this sensor.

Table A15. Main characteristics of the alternative stress energy transmitter a_{GV} .

Characteristic		Value
Measurement range	SEL kHz	0 ... 10 4 ... 50
Transverse sensitivity	%	<5

Appendix A.4.5. Absolute Turbine Bearing Vibration $a_{THB_{x,y}}$

In this case, the additional acceleration sensors have been mounted at the turbine bearing casing to validate the existing velocity sensors of the machine diagnosis system. Both sensors are placed very close to each other in order to check the signal quality and resolution. The used acceleration sensor was of the same type as the draft tube vibration one with the characteristic according to Table A13.

Appendix A.4.6. Shaft Torque T , Speed N , and Mechanical Power P_{mech}

One part of the overall instrumentation was dedicated to the measurement of torque and speed with subsequent determination of the mechanical power, which are associated with the functional performance of the turbine set. The system used provides an insight into these important machine parameters by using the shaft twist angle as measurement parameter. The system uses two optical fork sensors for the twist angle measurement. The application of the sensors at the hydropower plant is shown in Figure A12, which is near the lower generator bearing, and in Figure A13, which is close to the turbine guide bearing. The distance between both sensors was 5 m. It is based on a counting algorithm, and therefore, needs an exact and rigid support for the sensor application as well as markings glued to the shaft.



Figure A12. Upper sensor installation below the lower generator bearing.



Figure A13. Lower sensor installation above the turbine guide bearing.

The installed optical sensors use a light beam in the frequency range of 500 kHz to measure the time difference of sensor passing the markings. Due to the adequate

distance between both sensors and the high measurement frequency, the system works in a nanosecond range to ensure a high resolution of measurement. The setup of the whole systems also enables the measurement of the speed and, subsequently, to derive the mechanical shaft power, as the latter is the product of torque and angular speed.

References

1. Doujak, E.; Stadler, S.; Fillinger, G.; Haller, F.; Maier, M.; Nocker, A.; Gaßner, J.; Unterluggauer, J. Fatigue Strength Analysis of a Prototype Francis Turbine in a Multilevel Lifetime Assessment Procedure Part I: Background, Theory and Assessment Procedure Development. *Energies* **2022**, *15*, 1148. [[CrossRef](#)]
2. Doujak, E.; Unterluggauer, J.; Fillinger, G.; Nocker, A.; Haller, F.; Maier, M.; Stadler, S. Fatigue Strength Analysis of a Prototype Francis Turbine in a Multilevel Lifetime Assessment Procedure Part II: Method Application and Numerical Investigation. *Energies* **2022**, *15*, 1165. [[CrossRef](#)]
3. Aliabadi, A.; Shamekhi, A. Von Karaman frequency excitation caused cracking of the Karun III Francis runner. In Proceedings of the HYDRO 2007, Granada, Spain, 15–18 October 2007.
4. Frunzäverde, D.; Muntean, S.; Mărginean, G.; Câmpian, V.; Marşavina, L.; Terzi, R.; Şerban, V. Failure analysis of a Francis turbine runner. In Proceedings of the 25th IAHR Symposium on Hydraulic Machinery and Systems, Timisoara, Romania, 20–24 September 2010; Volume 12, p. 12115.
5. Gagnon, M.; Tahan, S.A.; Bocher, P.; Thibault, D. The role of high cycle fatigue (HCF) onset in Francis runner reliability. *IOP Conf. Ser. Earth Environ. Sci.* **2012**, *15*, 22005. [[CrossRef](#)]
6. Liang, Q.; Lais, S.; Gentner, C.; Braun, O.; Liang, Q.W. Efficient runner safety assessment during early design phase and root cause analysis. In Proceedings of the 26th IAHR Symposium on Hydraulic Machinery and Systems, Beijing, China, 19–23 August 2012; Volume 15, p. 52009. [[CrossRef](#)]
7. Amini, A.; Vagnoni, E.; Favrel, A.; Yamaishi, K.; Müller, A.; Avellan, F. Upper part-load instability in a reduced-scale Francis turbine: An experimental study. *Exp. Fluids* **2023**, *64*, 118. [[CrossRef](#)]
8. Trivedi, C.; Cervantes, M.J.; Gandhi, B.K.; Dahlhaug, O.G. Experimental and Numerical Studies for a High Head Francis Turbine at Several Operating Points. *J. Fluids Eng.* **2013**, *135*, 111102. [[CrossRef](#)]
9. Nennemann, B.; Morissette, J.F.; Chamberland-Lauzon, J.; Monette, C.; Braun, O.; Melot, M.; Coutu, A.; Nicolle, J.; Giroux, A.M. Challenges in Dynamic Pressure and Stress Predictions at No-Load Operation in Hydraulic Turbines. *IOP Conf. Ser. Earth Environ. Sci.* **2014**, *22*, 32055. [[CrossRef](#)]
10. Trivedi, C.; Gandhi, B.K.; Cervantes, M.J.; Dahlhaug, O.G. Experimental investigations of a model Francis turbine during shutdown at synchronous speed. *Renew. Energy* **2015**, *83*, 828–836. [[CrossRef](#)]
11. Østby, P.T.; Billdal, J.T.; Sivertsen, K.; Haugen, B.; Dahlhaug, O.G. Dynamic Stresses In High Head Francis Turbines. *Int. J. Hydropower Dams* **2016**, *23*, 88–92.
12. Weber, W.; Locquenghien, F.v.; Conrad, P.; Koutnik, J. Dynamic stresses in a Francis model turbine at deep part load. In Proceedings of the HYPERBOLE Symposium, Porto, Portugal, 2–3 February 2017; Avellan, F., Silva, B., Moreira, C., Eds.; IOPScience: Bristol, UK, 2017; Volume 813, p. 012014.
13. Carl, B.W. Dynamic Loads on Francis Turbines: An Experimental Study. Ph.D. Thesis, Norwegian University of Science and Technology (NTNU), Trondheim, Norway, 2019.
14. Zhang, L.; Feng, F.; Fan, X.; Jiang, P. Reliability analysis of Francis turbine blade against fatigue failure under stochastic loading. In Proceedings of the 2012 International Conference on Quality, Reliability, Risk, Maintenance and Safety Engineering: ICQR2MSE 2012, Chengdu, China, 15–18 June 2012; Huang, H.Z., Zuo, M.J., Liu, Y., Eds.; IEEE: Piscataway, NJ, USA, 2012; pp. 987–990.
15. Seidel, U.; Mende, C.; Hübner, B.; Weber, W.; Otto, A. Dynamic loads in Francis runners and their impact on fatigue life. In Proceedings of the IOP Conference Series: Earth and Environmental Science, Jakarta, Indonesia, 23–24 January 2014; Volume 22, p. 032054.
16. Huang, X.; Chamberland-Lauzon, J.; Oram, C.; Klopfer, A.; Ruchonnet, N. Fatigue analyses of the prototype Francis runners based on site measurements and simulations. In Proceedings of the 27th IAHR Symposium on Hydraulic Machinery and Systems, Montreal, QC, Canada, 22–26 September 2014; Volume 22, p. 12014. [[CrossRef](#)]
17. Unterluggauer, J.; Eichhorn, M.; Doujak, E. Fatigue analysis of Francis turbines with different specific speeds using site measurements. In Proceedings of the 19th International Seminar on Hydropower Plants, Wien, Austria, 14–16 November 2022; Technische Universität Wien: Wien, Austria, 2016; pp. 645–654.
18. Unterluggauer, J.; Doujak, E.; Bauer, C. Fatigue analysis of a prototype Francis turbine based on strain gauge measurements. *Wasserwirtsch. Extra* **2019**, *109*, 66–71. [[CrossRef](#)]
19. Trivedi, C.; Gandhi, B.; Cervantes, M.J. Effect of transients on Francis turbine runner life: A review. *J. Hydraul. Res.* **2013**, *51*, 121–132. [[CrossRef](#)]
20. Trivedi, C.; Cervantes, M.J. Fluid–structure interactions in Francis turbines: A perspective review. *Renew. Sustain. Energy Rev.* **2017**, *68*, 87–101. [[CrossRef](#)]
21. Egusquiza, E.; Valentín, D.; Presas, A.; Valero, C. Overview of the experimental tests in prototype. In Proceedings of the HYPERBOLE Symposium, Porto, Portugal, 2–3 February 2017; Avellan, F., Silva, B., Moreira, C., Eds.; IOPScience: Bristol, UK, 2017; Volume 813, p. 012037.

22. Zhang, Y.; Liu, K.; Xian, H.; Du, X. A review of methods for vortex identification in hydroturbines. *Renew. Sustain. Energy Rev.* **2018**, *81*, 1269–1285. [[CrossRef](#)]
23. Valentín, D.; Presas, A.; Bossio, M.; Egusquiza, M.; Egusquiza, E.; Valero, C. Feasibility of Detecting Natural Frequencies of Hydraulic Turbines While in Operation, Using Strain Gauges. *Sensors* **2018**, *18*, 174. . [[CrossRef](#)] [[PubMed](#)]
24. Titschkau, M.; Hasmatuchi, V.; Decaix, J.; Münch-Alligné, C. On-board measurements at a 100 MW high-head Francis turbine. In Proceedings of the 20th International Seminar on Hydropower Plants, Wien, Austria, 14–16 November 2022; Technische Universität Wien: Wien, Austria, 2018; pp. 385–396.
25. *ISO 20816-1:2016*; Mechanical Vibration—Measurement and Evaluation of Machine Vibration—Part 1: GENERAL Guidelines. DIN Deutsches Institut für Normung e.V.—German Standards: Berlin, Germany, 2016
26. *ISO 20816-5:2018*; Mechanical Vibration—Measurement and Evaluation of Machine Vibration—Part 5: Machine Sets in Hydraulic Power Generating and Pump-Storage Plants. DIN Deutsches Institut für Normung e.V.—German Standards: Berlin, Germany, 2018.
27. Doujak, E.; Unterluggauer, J. Fluid–structure interactiona of Francis turbines at different load steps. In Proceedings of the 9th International Symposium on Fluid-Structure Interactions, Flow-Sound Interactions, Flow-Induced Vibration & Noise, Toronto, BC, Canada, 8–11 July 2018.
28. Unterluggauer, J.; Sulzgruber, V.; Doujak, E.; Bauer, C. Experimental and numerical study of a prototype Francis turbine startup. *Renew. Energy* **2020**, *157*, 1212–1221. [[CrossRef](#)]
29. Unterluggauer, J.; Maly, A.; Doujak, E. Investigation on the Impact of Air Admission in a Prototype Francis Turbine at Low-Load Operation. *Energies* **2019**, *12*, 2893. [[CrossRef](#)]
30. Unterluggauer, J.; Doujak, E.; Bauer, C. Fatigue analysis of a Francis turbine based on strain gauge measurements. In Proceedings of the 20th International Seminar on Hydropower Plants, Wien, Austria, 14–16 November 2018; Technische Universität Wien: Wien, Austria, 2018. ISBN 978-3-9504338-1-4.
31. Mühlbacher, K. Evaluation and Analysis of Measurement Data of a Francis Turbine. Master’s Thesis, TU Wien, Wien, Austria, 2019.
32. Eichhorn, M.; Taruffi, A.; Bauer, C. Expected load spectra of prototype Francis turbines in low-load operation using numerical simulations and site measurements. *J. Phys. Conf. Ser.* **2017**, *813*, 012052. . [[CrossRef](#)]
33. Gaßner, E.; Buxbaum, O.; Ostermann, H.; Rückert, H. Ausfallsichere Bemessung von Laufrädern für Wasserkraftmaschinen aus rostfreiem Stahlguss unter Berücksichtigung von Korrosion und Gefügestand. In *Abschlussbericht zum Gemeinschaftsprogramm “Stahlguss”*; BMFT-Industrie-LBF, Fraunhofer-Institute für Betriebsfestigkeit: Darmstadt, Germany, 1983.
34. FKM Forschungskuratorium Maschinenbau e.V. *Analytical Strength Assessment of Components: FKM Guideline 7th Edition 2020*, 7th ed.; VDMA: Frankfurt, Germany, 2021; ISBN 978-3-8163-0745-7.
35. Unterluggauer, J. Lifetime Calculation of a Francis Turbine from Data of a Prototype Measurement. Master’s Thesis, TU Wien, Wien, Austria, 2016.
36. Miner, M.A. Cumulative Damage in Fatigue. *J. Appl. Mech.* **1945**, *12*, 159–164. [[CrossRef](#)]
37. *IEC 60041:1991*; Field Acceptance Tests to Determine the Hydraulic Performance of Hydraulic Turbines, Storage Pumps and Pump-Turbines. International Electrotechnical Commission: Geneva, Switzerland, 1991.
38. Eichhorn, M.; Doujak, E.; Schübl, A. Cavitation measurements in hydraulic machines by using accelerometers. *Wasserwirtsch. Extra* **2015**, *105*, 89–93. [[CrossRef](#)]

Disclaimer/Publisher’s Note: The statements, opinions and data contained in all publications are solely those of the individual author(s) and contributor(s) and not of MDPI and/or the editor(s). MDPI and/or the editor(s) disclaim responsibility for any injury to people or property resulting from any ideas, methods, instructions or products referred to in the content.